SURFACE PLASMON BASED ENHANCED TRANSMISSION OF ELECTROMAGNETIC WAVES

A THESIS
SUBMITTED TO THE DEPARTMENT OF PHYSICS
AND THE INSTITUTE OF ENGINEERING AND SCIENCE
OF BİLKENT UNIVERSITY
IN PARTIAL FULFILLMENT OF THE REQUIREMENTS
FOR THE DEGREE OF
MASTER OF SCIENCE

By

Süheyla Sena Akarca Bıyıklı

July 2004

I certify that I have read this thesis and that in my opinion it is fully adequate, in scope and in quality, as a dissertation for the degree of Master of Science.

Prof. Dr. Ekmel Özbay (Supervisor)

I certify that I have read this thesis and that in my opinion it is fully adequate, in scope and in quality, as a dissertation for the degree of Master of Science.

Prof. Dr. Atilla Erçelebi

I certify that I have read this thesis and that in my opinion it is fully adequate, in scope and in quality, as a dissertation for the degree of Master of Science.

Assist. Prof. Özgür Aktaş

Approved for the Institute of Engineering and Science:

Prof. Mehmet Baray,
Director of the Institute of Engineering and Science

Abstract

SURFACE PLASMON BASED ENHANCED TRANSMISSION OF ELECTROMAGNETIC WAVES

Süheyla Sena Akarca Bıyıklı
M. S. in Physics
Supervisor: Prof. Ekmel Özbay
July 2004

Grating-coupling phenomena between surface plasmons and electromagnetic waves are studied in the microwave spectrum using metallic gratings. Transmission and reflection measurements were carried out to observe the transmitted and reflected radiation around the surface plasmon resonance frequencies. Grating structures with subwavelength apertures were designed for transmission experiments. Measurements were done in the microwave spectrum of 10–37.5 GHz, corresponding to a wavelength region of 8–30 mm. The Al samples had a grating periodicity of 16 mm. A 2 mm-wide subwavelength slit was opened for transmission samples. Samples with one/double-sided gratings displayed remarkably enhanced transmission and directivity with respect to the reference sample without gratings. The experimental results agreed well with theoretical

simulations. ~50% transmission at 20.7 mm, ~25-fold enhancement, and ±4° angular divergence was achieved with a ~λ/10 aperture. Reflection measurements of one-sided grating sample resulted in clear observation of surface plasmon coupling phenomena. Reflectivity peaks were measured around theoretically calculated resonance frequencies.

Keywords: surface plasmon, extraordinary transmission, plasmon coupling, 1-D grating structures, subwavelength aperture, microwave radiation, transmission, reflection, directivity

Özet

ELEKTOMANYETİK DALGALARIN YÜZEY PLAZMON TABANLI ARTTIRILMIŞ İLETİMİ

Süheyla Sena Akarca Bıyıklı
Fizik Yüksek Lisans
Tez Yöneticisi: Prof. Ekmel Özbay
Temmuz 2004

Yüzey plazmonları ile elektromanyetik dalgalar arasındaki ızgara-bağlama hadisesi metalik ızgara yapıları kullanılarak mikrodalga spektrumunda incelendi. Yüzey plazmon rezonans frekansları civarındaki geçen ve yansıyan radyasyonun davranışını gözlemlemek için spektral geçirgenlik ve yansıma ölçümleri yapıldı. Geçirgenlik deneyleri için dalgaboyu-altı yarıklara sahip ızgara yapıları tasarlandı. Ölçümler 10–37.5 GHz mikrodalga frekans aralığında (8–30 mm dalgaboyu aralığına karşılık geliyor) yapıldı. Metalik Al örneklerin ızgara periyodu 16 mm olarak tasarlandi. Geçirgenlik ölçümünde kullanılacak örneklerde 2 mm genisliğinde dalgaboyu-altı yarık açıldı. Tek/çift taraflı ızgara örnekleri ızgarasız

referans örneğiyle karşılaştırıldığında oldukça arttırılmış geçirgenlik ve açısal yönlendirme yeteneği sergiledikleri gözlemlendi. Deney sonuçları kuramsal simulasyonlar ile yakın uyum gösterdi. ~λ/10 genişliğe sahip bir yarık ile 20.7 mm'de ~50% geçirgenlik, ~25 kat artırım ve ±4° ayrılma açısı elde edildi. Tek taraflı ızgara yapıları ile yapılan yansıma ölçümleri, yüzey plazmon bağlama hadisesini açıkça doğrulayan gözlem sonuçları verdi. Ölçülen yansıma spektrumunun tepe noktaları kuramsal olarak hesaplanan rezonans frekanslarına çok yakın noktalarda çıktı.

Anahtar Sözcükler: yüzey plazmonu, artırılmış geçirgenlik, plazmon bağlama, 1-D ızgara yapıları, dalgaboyu-altı yarık, mikrodalga radyasyon, geçirgenlik, yansıma, yönlendirme

Acknowledgements

It is my pleasure to express my sincere gratitude to my supervisor Prof. Ekmel Özbay for his invaluable guidance, motivation, encouragement, confidence and understanding. I learned a lot from his superior academic personality and he will always be a model for my academic career.

I also thank the members of the thesis committee, Prof. Atilla Erçelebi and Asst. Prof. Özgür Aktaş for their useful comments and suggestions.

I would especially like to thank İrfan Bulu for his computational skills, helping in the numerical calculation part of this work.

I would like to thank all members of Advanced Research Laboratory for their continuous support. Thank you all, members of the Physics Department for making life easier and enjoyable. I want to especially thank the group members of the photonic research team: Kaan Güven, Koray Aydın, İrfan Bulu and Hümeyra Çağlayan. It was a pleasure to work with these hard-working friends in the same group.

Finally I would express my endless thank to my family for their understanding and continuous moral support. Very special thanks belong to my husband, Necmi, for his endless moral support, encouragement, understanding, and love.

Contents

List of Figures

List of Tables

Chapter 1

Introduction

Surface plasmons (SPs) can be described as fluctuations of the surface electron density on metallic surfaces. These charge density waves can be characterized by intense electromagnetic fields confined to the surface. The strength of the electromagnetic fields decay exponentially as one moves away from the surface, but they vary in wavelike fashion as one moves parallel to the surface [1]. SP modes have longer wave vectors than light waves of the same energy. Therefore, SP waves are non-radiative, and cannot propagate in non-metallic media [2]. SPs have an extensive history as they emerged as solutions of Maxwell equations at an interface. However, interest in SPs increased only after late 1960s when prism coupling was established as a method to couple free propagating light to SPs [2],[38]. Another way to excite SPs is the grating coupling technique, in which the incident radiation is coupled to SPs using periodic surface corrugation [2]. Many application fields aroused by using the coupling property of SPs [4]-[7].

In 1998, Ebbesen *et al.* demonstrated extraordinary optical transmission (EOT) through subwavelength hole array structures [8]. According to standard diffraction theory, subwavelength apertures transmit light very poorly and diffract in all directions uniformly [9]. Afterwards, many theoretical and experimental studies on EOT through subwavelength apertures (holes or slits) proved that this phenomenon was due to resonant excitation of SPs by a periodic array on the surface [10]-[26]. Different metal types [21], groove

periodicity [11]-[13], [20], groove depth [12], [14] and aperture shapes [27] were used to analyze the EOT phenomena. 1-D [10]-[19] and 2-D [20]-[26] periodic surface corrugations were implemented in these studies. The optical beaming property of subwavelength apertures in metallic grating structures was reported [17] and theoretically explained [18]. In another study, enhanced transmission through subwavelength hole arrays was shown at THz frequencies [28].

Hibbins *et al* recently carried out similar studies at the microwave frequency level. Using grating structures, they demonstrated the coupling of microwave radiation to SPs by reflection measurements [29]-[32]. They have also presented microwave transmission enhancement through a subwavelength slit without grating [33]. Very recently, Lockyear *et al*. reported an enhanced transmission at microwave frequencies through circular subwavelength aperture surrounded by periodic concentric grooves [34].

In this work, we experimentally and theoretically demonstrate transmission enhancement and beaming of microwave radiation through a subwavelength slit surrounded by periodic gratings. Reflection measurements have also been carried out to observe resonant SP excitation.

In Chapter 2, the plasma concept is introduced, then basic properties of surface plasmons are obtained by solving Maxwell equations at the metal-dielectric interface. At the end of this chapter, excitation of non-radiative surface plasmons is explained by way of three different methods.

In the third chapter, we present the designed samples used in our experiments. 5 samples were designed for transmission experiments, 2 samples were prepared for reflection studies. We also briefly describe the simulation technique used for our calculations.

In the fourth chapter, experimental setups and results of measurements and simulations are presented. The transmission results are compared with the theoretical calculations. Thereafter for better understanding of the surface plasmon coupling effect we present the reflection measurements.

The thesis concludes with the summary of our measurements and achievements, and possible future research directions.

Chapter 2

Theoretical Background

A theoretical description of surface plasmons at an interface formed by a metal and a dielectric is based on Maxwell's equations. In this chapter, we first introduce the plasma concept in metals. Afterwards, with the help of Maxwell's equations, the electromagnetic field of the surface plasmon propagating along the metal-dielectric interface is derived. Finally, the excitation methods of non-radiative surface plasmons are presented.

2.1 Plasma Concept

One of the approaches to derive the properties of the solid state is the plasma concept: the free electrons of a metal are treated as an electron liquid of high density of about 10^{23} cm^{-3}.

By this approach the dielectric function for metals can be calculated [35]. The long wavelength dielectric response $\varepsilon(\omega)$ of an electron gas is obtained from the equation of motion of a free electron in an electric field:

$$m\frac{d^2x}{dt^2} = -eE \tag{2.1}$$

If x and E have the time dependence $e^{-i\omega t}$, then

$$-\omega^2 mx = -eE\ ; \qquad x = eE/m\omega^2 \tag{2.2}$$

and the polarization , defined as the dipole moment per unit volume, is

$$P = -nex = -\frac{ne^2}{m\omega^2}E \tag{2.3}$$

where n is the electron concentration.

The dielectric function at frequency ω is

$$\varepsilon(\omega) = \frac{D(\omega)}{E(\omega)} = 1 + 4\pi \frac{P(\omega)}{E(\omega)}; \tag{2.4}$$

From equations 2.3 and 2.4, the dielectric function of the electron gas

$$\varepsilon(\omega) = 1 - \frac{4\pi n e^2}{m\omega^2} \tag{2.5}$$

This equation can be written as:

$$\varepsilon(\omega) = 1 - \frac{\omega_p^2}{\omega^2} \tag{2.6}$$

where ω_p, plasma frequency is defined by the relation

$$\omega_p^2 = 4\pi n e^2 / m \tag{2.1}$$

A plasma oscillation in a metal is a collective longitudinal excitation of the conduction electron gas. These plasma oscillations propagate through the volume of the metal. Plasmon is a quantum of a plasma oscillation, that has the energy $\hbar\omega_p$.

2.2 Plasmons at an interface: Surface Plasmons

The electron charges on a metal boundary perform fluctuations that are called surface plasma oscillations [2].

Now, we will find the wave vector of these surface waves and calculate the dispersion relation:

We consider the plane interface between two semi-infinite media. Medium 1 and medium 2 have the dielectric permittivities of ε_1 and ε_2, respectively. We take the x axis as the propagation direction, and the z axis as normal to the interface, which is shown in figure 2.1.

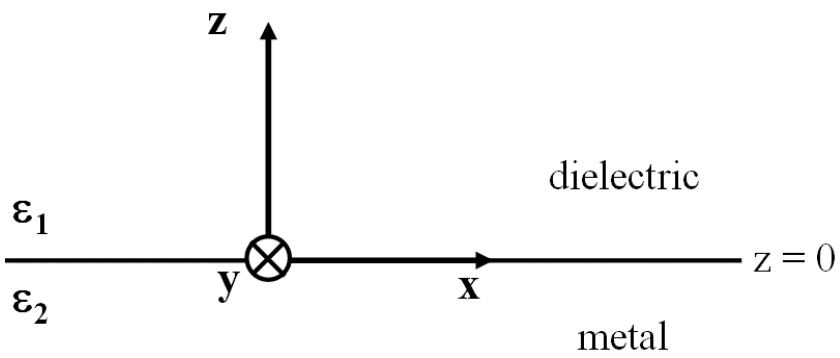

Fig. 2.1: Schematic description of coupling free electromagnetic waves to SPs by grating that has a period of λ_g

Field equations in two media are given by:

$$z > 0 \qquad \begin{aligned} \mathbf{H_1} &= (0, H_{y1}, 0)\exp i(k_{x1}x + k_{z1}z - \omega t) \\ \mathbf{E_1} &= (E_{x1}, 0, E_{z1})\exp i(k_{x1}x + k_{z1}z - \omega t) \end{aligned} \tag{2.8}$$

$$z < 0 \qquad \begin{aligned} \mathbf{H_2} &= (0, H_{y2}, 0)\exp i(k_{x2}x - k_{z2}z - \omega t) \\ \mathbf{E_2} &= (E_{x2}, 0, E_{z2})\exp i(k_{x2}x - k_{z2}z - \omega t) \end{aligned} \tag{2.9}$$

These fields have to comply with Maxwell's equations:

$$\nabla \times \mathbf{H}_i = \varepsilon_i \frac{1}{c}\frac{\partial}{\partial t} E_i \tag{2.10}$$

$$\nabla \times \mathbf{E}_i = -\frac{1}{c}\frac{\partial}{\partial t} H_i \tag{2.11}$$

$$\nabla \cdot \varepsilon_i \mathbf{E}_i = 0 \tag{2.12}$$

$$\nabla \cdot \mathbf{H}_i = 0 \tag{2.13}$$

And the continuity equations,

$$E_{x1} = E_{x2} \tag{2.14}$$

$$H_{y1} = H_{y2} \tag{2.15}$$

$$\varepsilon_1 E_{z1} = \varepsilon_2 E_{z2} \tag{2.16}$$

From equations (2.14) and (2.15),

$$k_{x1} = k_{x2} = k_x \tag{2.17}$$

Equation (2.10) gives

$$\frac{\partial H_{yi}}{\partial z} = -\varepsilon_i E_{xi} \frac{\omega}{c} \quad \Rightarrow \quad \begin{aligned} k_{z1} H_{y1} &= -\frac{\omega}{c} \varepsilon_1 E_{x1} \\ k_{z2} H_{y2} &= \frac{\omega}{c} \varepsilon_2 E_{x2} \end{aligned} \tag{2.18}$$

Equation (2.18) together with (2.14,15) yield

$$\frac{k_{z1}}{\varepsilon_1} H_{y1} + \frac{k_{z2}}{\varepsilon_2} H_{y2} = 0 \tag{2.19}$$

To obtain a solution, the determinant D_0 has to be zero

$$D_0 = \frac{k_{z1}}{\varepsilon_1} + \frac{k_{z2}}{\varepsilon_2} = 0 \tag{2.20}$$

This is the dispersion relation for the system in Fig.2.1.that we obtain from (2.10,11,18)

$$k_x^2 + k_{zi}^2 = \varepsilon_i \left(\frac{\omega}{c} \right)^2 \tag{2.21}$$

From (2.20) together with (2.21) gives the dispersion relation for surface waves,

$$k_x = \frac{\omega}{c} \left(\frac{\varepsilon_1 \varepsilon_2}{\varepsilon_1 + \varepsilon_2} \right)^{1/2} \tag{2.22}$$

Equation (2.20) shows that for the surface plasmon to exist, ε_1 and ε_2 must have opposite signs:

$$\varepsilon_1 \varepsilon_2 < 0 \tag{2.23}$$

Also from equation (2.22)

$$\varepsilon_1 + \varepsilon_2 < 0 \tag{2.24}$$

In our experiments, medium 1 is always air ($\varepsilon_1 = 1$). Then, ε_2 must be negative and $\varepsilon_2 < -\varepsilon_1$. medium 2 is then called the *surface-active* medium [3].

To illustrate the results, the dispersion curve for SPs is shown (Fig. 2.2). It can be seen that, the dispersion relation approaches the light line at small k_x , but remains larger, so that the SPs cannot transform into light. Thus SPs are nonradiative surface waves. At large k_x the value of ω approaches,

$$\omega_{SP} = \frac{\omega_p}{\sqrt{\varepsilon_1 + 1}} \tag{2.25}$$

For air-metal interface,

$$\omega_{SP} = \frac{\omega_p}{\sqrt{2}} \tag{2.26}$$

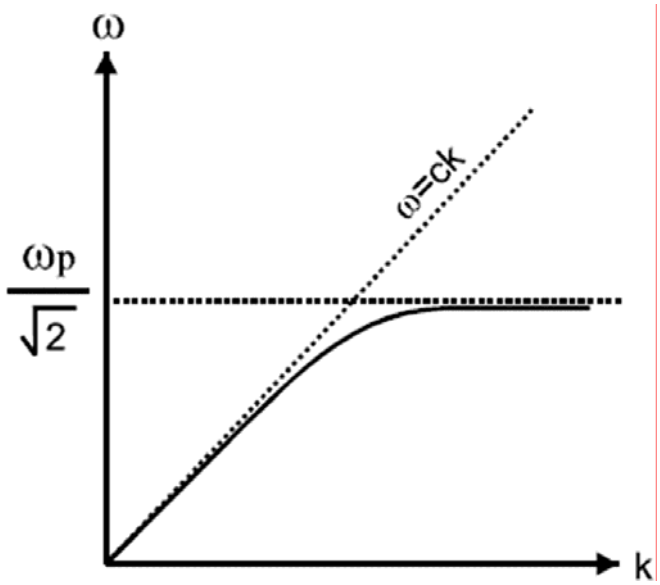

Fig. 2.2: Dispersion diagram for SPs on a planar metal-air interface. Dotted line shows the dispersion of light in free-space

2.3 Excitation of Surface Plasmons

As it is explained in the previous section, surface plasmons are nonradiative since the dispersion relation lies to the right of the light line ($k_x > \omega/c$). For excitation at a given frequency, the wave vector of the radiation has to be increased by Δk_x [2]. Coupling between propagating waves and surface evanescent waves requires additional techniques, some of which shall be presented in this section. All of these techniques have in common that they can be used for coupling free electromagnetic radiation with surface evanescent waves (incoupling) or vice versa (outcoupling).

2.3.1 Aperture coupling

The aperture coupling technique allows a broadband coupling for a continuum of frequencies. In this method, radiation comes to the surface of the sample with an angle θ with respect to the normal of the surface. Radiation is focused to a small gap that is defined by the sample surface and the edge of a razor blade. The geometry leads to a scattering of the incident radiation and the generation of evanescent waves comprising a continuum of wave vectors. As a consequence, the dispersion relations of a fraction of the incident radiation and the SPs match, i.e., coupling becomes possible. The maximum coupling efficiency of this method has been reported to be 10% for field amplitudes [37].

2.3.2 Prism coupling

The basic principle of this method is coupling SPs with the evanescent waves formed by total internal reflection. A prism is placed above the metal surface. A radiation is incident with an angle greater than critical angle, so that total internal reflection(TIR) occurs. TIR requires the evanescent modes, which have greater wave vector than the incident radiation. The tail of the evanescent mode can excite a surface mode on the metal surface [38],[39]

.

2.3.3 Grating coupling

If light hits a metal grating with a grating period λ_g , at an angle θ, the wave vector of the incident radiation along the grating surface is calculated by:

$$k_{//} = \frac{\omega}{c}\sin\theta \pm nk_g \tag{2.23}$$

Where n is an integer and $k_g = 2\pi/\lambda_g$. If $k_{//}$ is equal to the wave vector of SP (Eq.2.22), then coupling occurs between the incident radiation and the SP.

$$\frac{\omega}{c}\sqrt{\frac{\varepsilon}{\varepsilon+1}} = k_{SP} = \frac{\omega}{c}\sin\theta \pm nk_g \tag{2.24}$$

Because the grating can provide impinging free waves with additional momentum arising from the grating periodic structure, the linear free wave dispersion relation changes into a set of straight lines which can then match the SP dispersion relation (Fig.2.3).

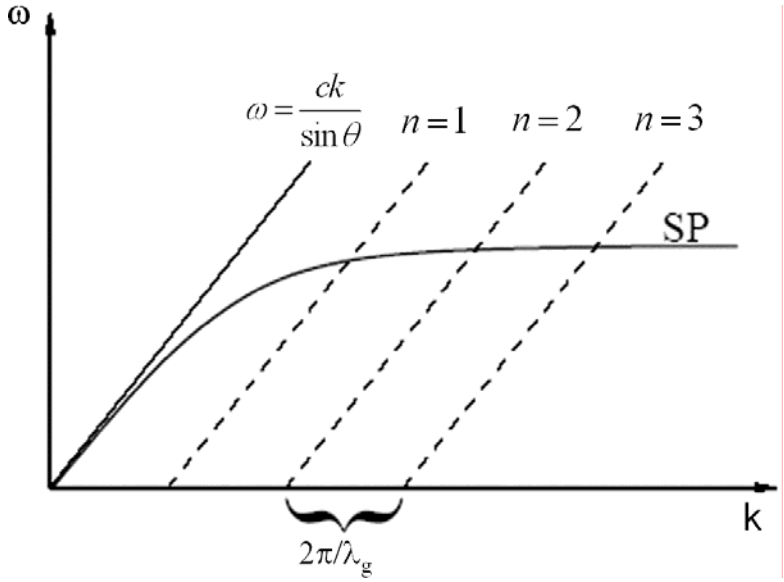

Fig. 2.3: Schematic description of coupling free electromagnetic waves to SPs by way of grating that has a period of λ_g

.

Chapter 3

Design and Simulation

In this chapter, the samples that will be analyzed are introduced. The design parameters are described. There is also an overview of the simulation tools.

3.1 Sample Design

We investigated SP properties at microwave frequencies for six different samples:

- Reference sample: Slit without any grating
- One-sided sinusoidal grating with a slit
- Double-sided sinusoidal grating with a slit
- Double-sided symmetric rectangular grating with a slit
- Double-sided asymmetric rectangular grating with a slit
- One-sided sinusoidal grating without slit

The first five samples were designed for transmission measurements, whereas the last sample (without slit) was designed for reflectivity experiments. All of the samples were metallic and made of aluminum (Al). The samples were fabricated using a CNC machine with a process resolution of 0.1 mm.

3.1.1 Reference Sample

The first sample was designed as a reference sample for transmission measurements. Since it was known that, apertures smaller than incident wavelength transmit very poorly and diffract light in all directions, the reference sample was a metal plate with a subwavelength slit in it. We studied in the 10-37.5 GHz frequency range, corresponding to a wavelength region of 8–30 mm. As can be seen in Fig. 3.1 thickness of the metallic plate and the slit width are 8mm and 2mm, respectively.

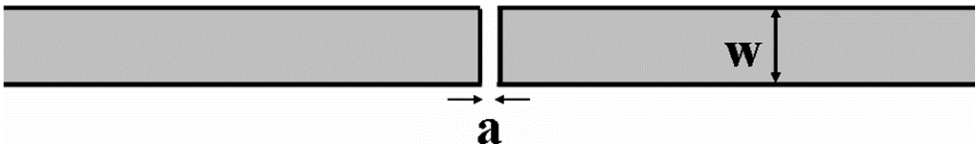

Fig. 3.1: Schematic picture of reference sample with a=2mm and w=8mm

3.1.2 One-Sided Grating

As it is explained in the theoretical background chapter, there are several ways to excite surface plasmons. Coupling by grating is one of them. So, as the next sample, we added sinusoidal grating on one surface of the metallic plate, around the slit (Fig. 3.2). According to the coupling formula:

$$\mathbf{k}_{SP} = n_d \mathbf{k}_0 \sin\theta \pm N\mathbf{k}_g$$

where $k_g=2\pi/\lambda_g$, period of the grating is important in coupling. It should not be greater or smaller than our study range (8mm-30mm). We chose 16mm for grating periodicity (λ_g). According to the previous studies by grating structures [2], [12] deeper groove depths (h) for grating produce better results.

As a result, our second sample was an aluminum plate with a slit and grating on one surface. Slit width was 2mm. Metal thickness is defined as the thickness that light passes through, which is 8 mm. Period of the grating was 16mm, groove depth was 4mm.

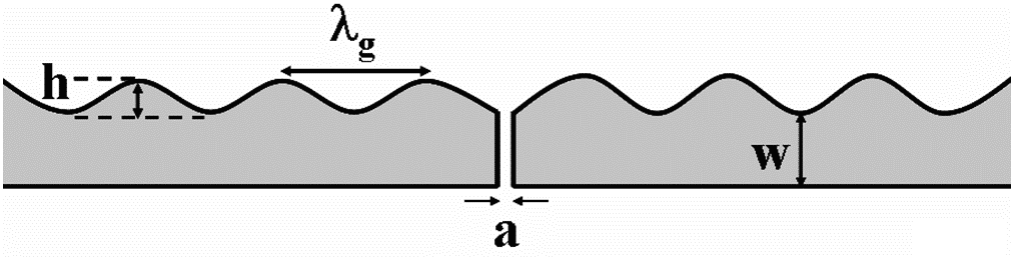

Fig. 3.2: Schematic diagram of one-sided grating sample with λ_g=16 mm, a=2 mm, w=8 mm, and h=4 mm.

3.1.3 Double-Sided Sinusoidal Grating

Recent studies in optical wavelengths showed that grating on the front surface enhances transmission and the grating on the back/exit surface gives directionality to the beam [17], [18]. Then, as the next sample we designed a metallic plate with grating on both surfaces. Parameters are shown in Fig. 3.3, as a 2mm slit width (a), 8 mm metal thickness (w), 16 mm grating period (λ_g), and 4mm groove depth (h).

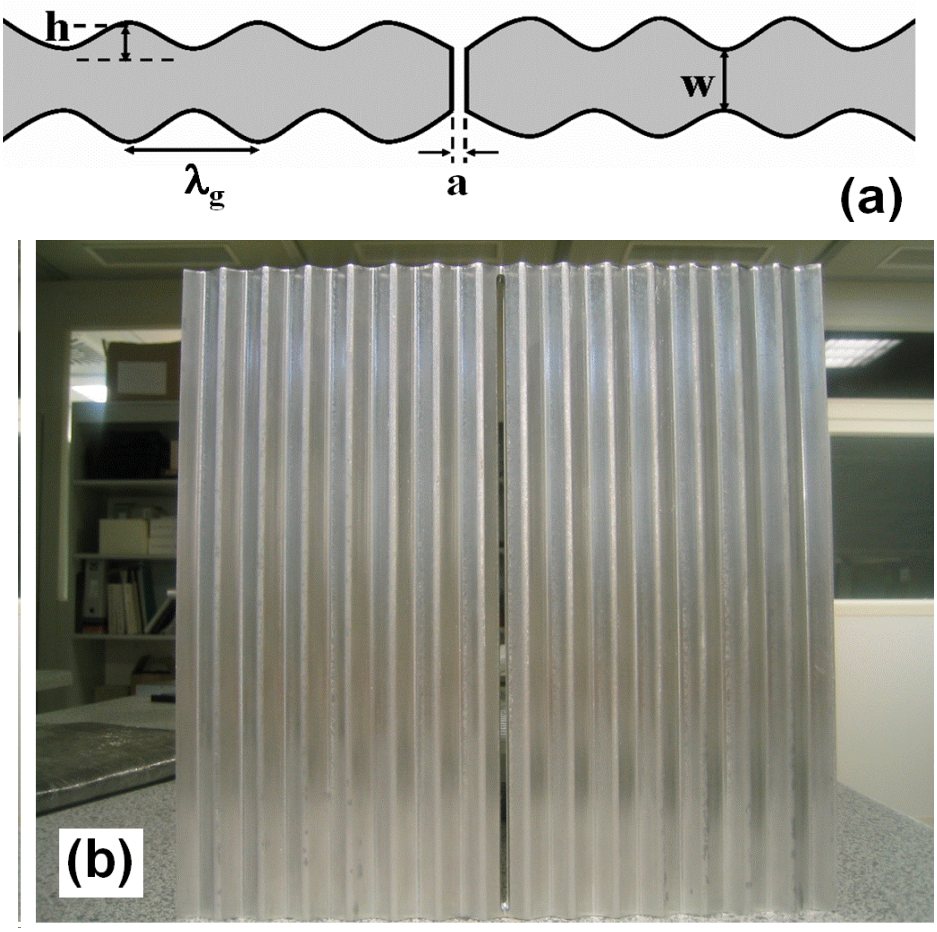

Fig. 3.3: (a) Schematic diagram of double-sided sinusoidal grating sample with λ_g=16 mm, a=2 mm, w=8 mm, and h=4 mm. (b) Photograph of the double-sided sinusoidal sample

3.1.4 Double-Sided Symmetric Rectangular Grating

Different shaped gratings were studied in different researches. To investigate the effect of grating shape, we designed two other samples. One of these was double-sided symmetric rectangular grating. Period of the grating, grating depth, slit width and slit thickness were the same as the sinusoidal sample. The grating shape was rectangular and the groove width (b) was 8 mm, half of the period. (Fig. 3.4)

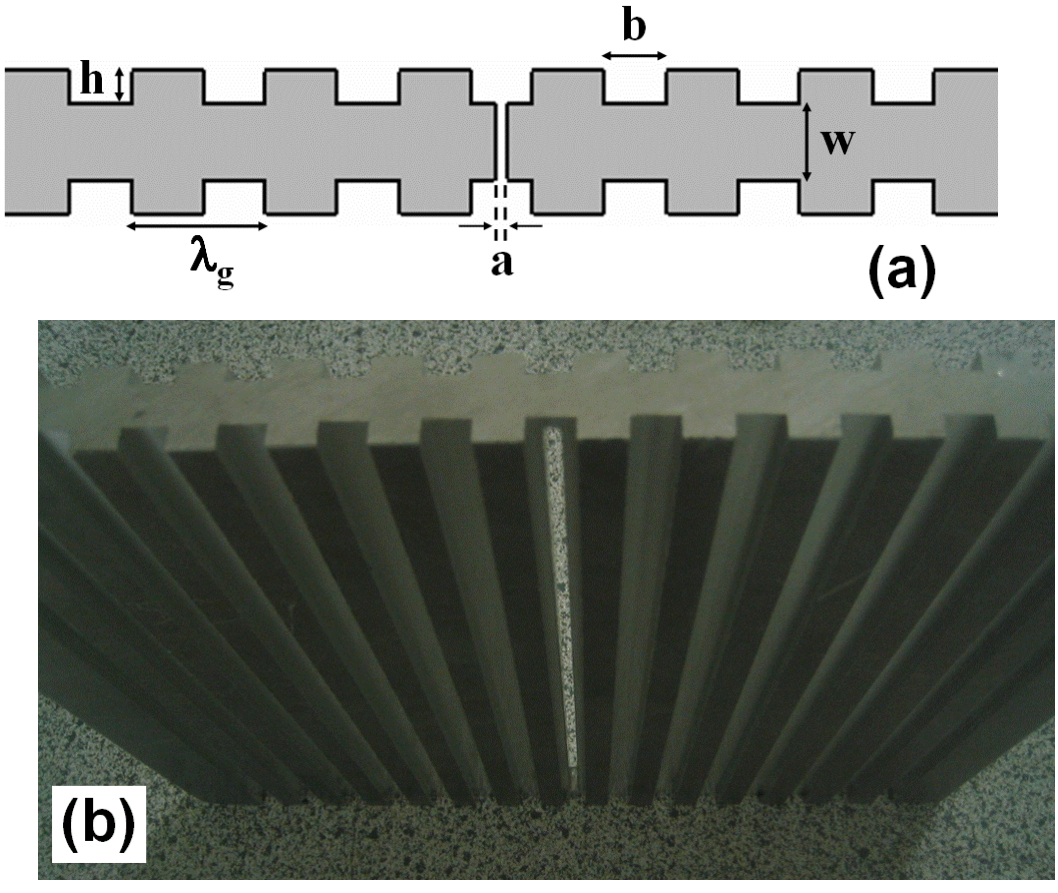

Fig. 3.4: (a) Schematic of double-sided symmetric rectangular grating sample with λ_g=16 mm, a=2 mm, b=8 mm, w=8 mm, and h=4 mm. (b) Photograph of symmetric rectangular grating

3.1.5 Double-Sided Asymmetric Rectangular Grating

The last sample for transmission measurements was again a double-sided grating sample. The period of the grating, grating depth, slit width are the same as the sinusoidal sample. Grating shape was rectangular, but the groove width (b) is 2mm that is equal to the slit width. For this sample the metal thickness (w) is 16 mm as can be seen in Fig. 3.5.

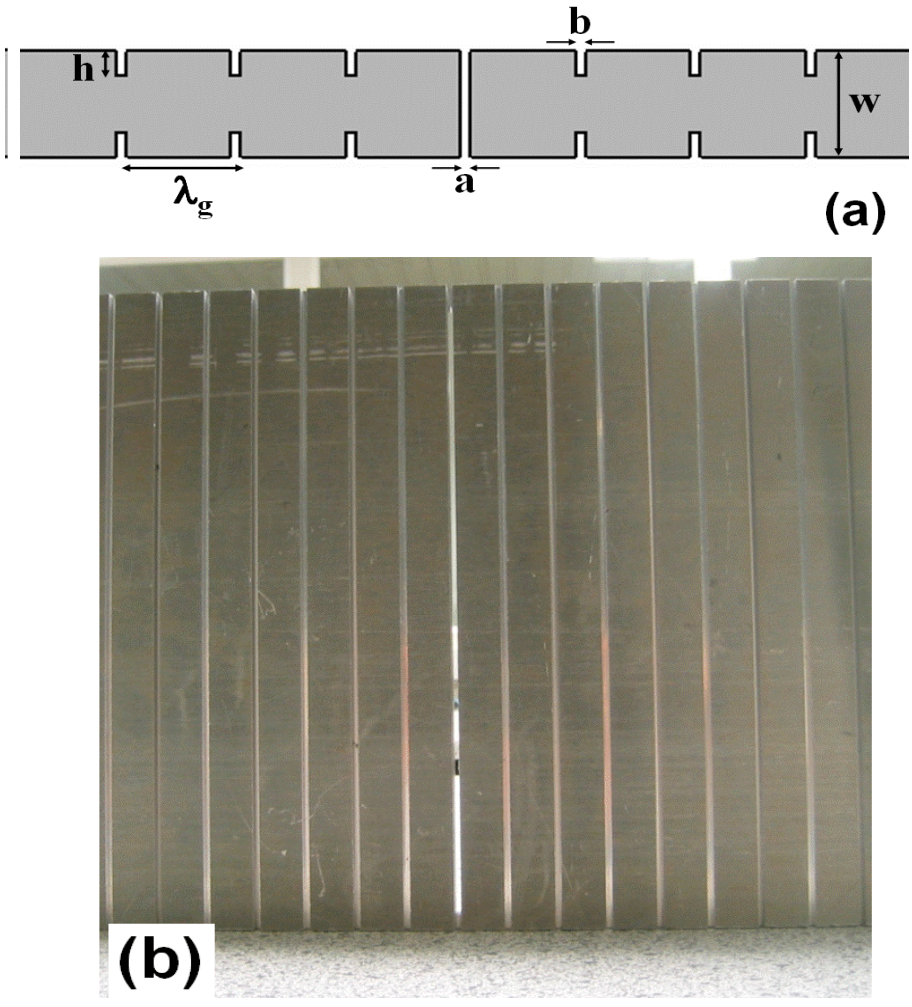

Fig. 3.5: (a) Schematic of double-sided symmetric rectangular grating sample with λ_g=16 mm, a=2 mm, b=2 mm, w=16 mm, and h=4 mm. (b) Photograph of sample

3.1.6 One-sided sinusoidal grating without slit

For reflectivity measurements, we designed a one-sided grating structure. There was no slit in the plate. The sample is a 240mm×240mm metallic plate that has sinusoidal grating on it. The period of the grating and groove depth are 16mm and 4mm, respectively (Fig.3.6).

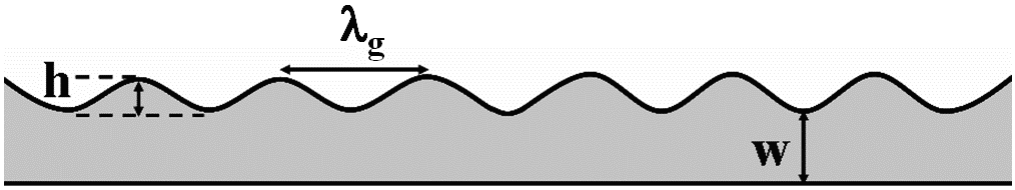

Fig. 3.6: Schematic diagram of one-sided sinusoidal grating sample with λ_g=16 mm, w=8 mm, and h=4 mm.

3.2 Simulation

Theoretical calculations were done using the finite-difference-time-domain (FDTD) method-based simulations. FDTD is a direct space-time approach. The basic algorithm of FDTD method depends on Maxwell's equations. When Maxwell's differential form equations are examined (Eq. (2.10),(2.11)), it can be seen that the time derivative of the E field is dependent on the Curl of the H field. Thus, the change in the E field (the time derivative) is dependent on the change in the H field across space (the Curl). This results in the basic FDTD equation that the new value of the E field is dependent on the old value of the E field (hence the difference in time) and the difference in the old value of the H field on either side of the E field point in space. The H field is found in the same manner. The new value of the H field is dependent on the old value of the

H field (hence the difference in time), as well as dependent on the difference in the E field on either side of the H field point.

In this method, an oscillating wave source is introduced into the grid and "directed" at the structure to be analyzed (Fig 3.7). The entire grid is then time-stepped until steady state response oscillations are obtained at all points on the grid. In order to use FDTD, a computational domain where the simulation will be performed must be established. The E and H fields will be determined at every point within the computational domain. The material (air, metal or dielectric) of each cell within the computational domain must be specified. Once the computational domain and the grid material are established, a source is specified. It is suitable to introduce a Gaussian pulse, to calculate the spectral response.

Since the E and H fields are determined directly, the output of the simulation is usually the E or H field at a point or a series of points within the computational domain.

To define structures, permittivity should be specified. Permittivity of free-space (air) is 1. The permittivity of metal depends on the frequency of the incident radiation. So, we modeled our structure by using the Drude dispersion model, which is one of the models to determine the frequency dependent permittivity of metals. Drude model assumes that, all of the conduction electrons can freely move around inside the metal to form a gas of non-interacting particles. The permittivity is given by the relation:

$$\varepsilon(\omega) = 1 - \frac{{\omega_p}^2}{\omega\left(\omega - i\omega_\tau\right)} \tag{2.25}$$

where ω_p =3570 THz is the plasma frequency, and ω_τ =19.4 THz is the absorption coefficient for aluminum [36].

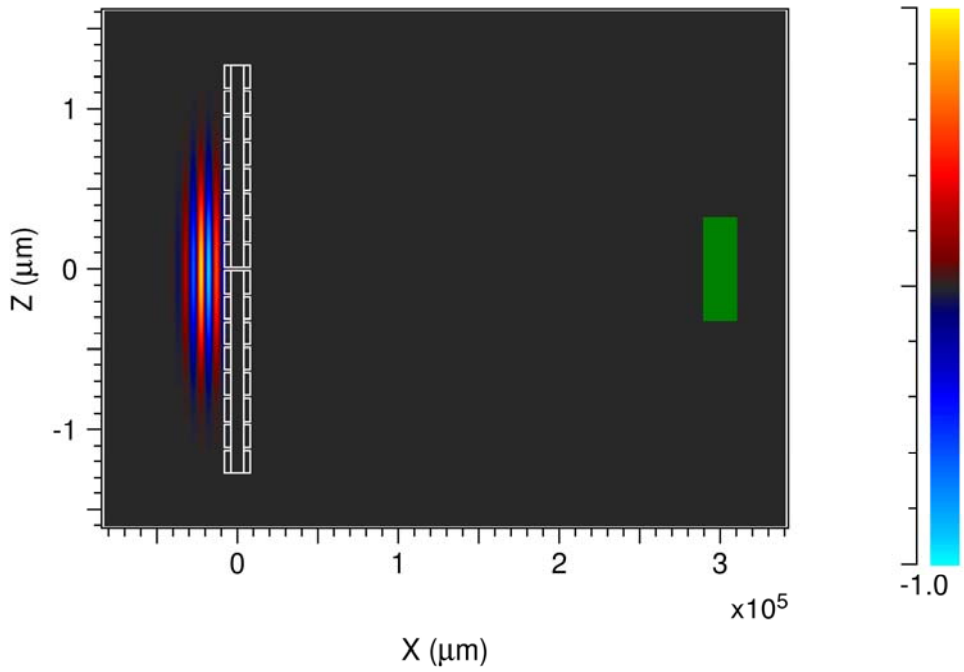

Fig. 3.7: View of simulation domain. A Gaussian beam is impinging on the sample, and the transmitted beam is recorded at 30 cm away from the sample.

Chapter 4

Measurements

After the design of samples, transmission measurements were conducted. In this chapter, we present the measurement setups, results of transmission measurements and simulation of each sample. The transmission results were discussed and compared. Then for better understanding of the surface plasmon coupling effect we present the reflection measurements.

4.1 Measurement Setup

Our experimental setup consists of a 50 GHz HP-8510C network analyzer and two horn antennas. The horn antennas were placed on rotating arms. The measurements were conducted in two frequency ranges: 10-20 GHz and 20-40 GHz. Antennas with horn sizes of 42×60 mm^2 and 29×42 mm^2 were utilized for these frequencies, respectively.

4.1.1 Setup for Transmission Measurements

Schematic description and a photograph of the setup are shown in Fig. 4.1. Both transmitter and receiver antennas were in TM mode, so that the electric field was perpendicular to the groove direction. In TE mode, the excitation of surface plasmons is not possible. The transmitter antenna was placed 15 cm away from the sample. Input radiation was normally incident upon the sample. Receiver

antenna was 30 cm away from the sample's back face and it was connected to a rotating arm to measure the angle dependence of the far-field radiation.

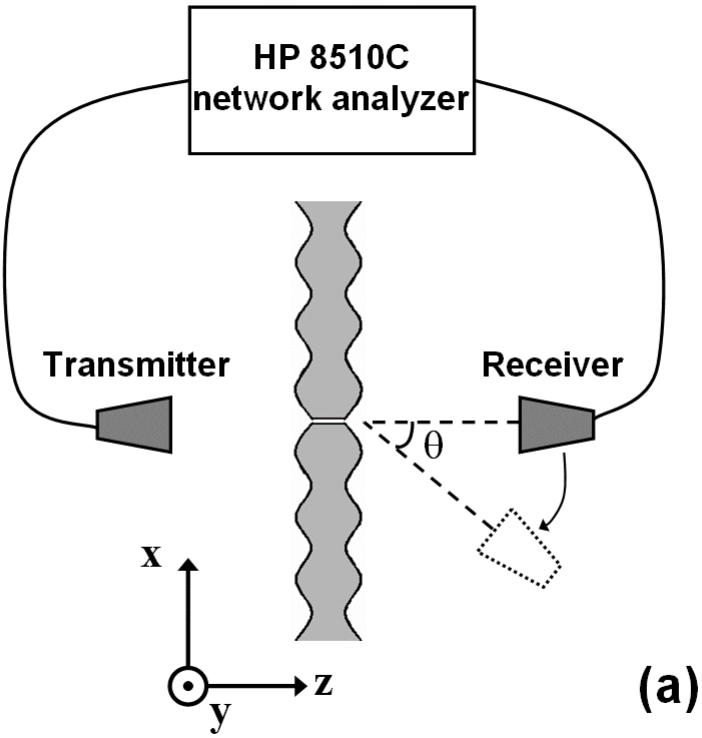

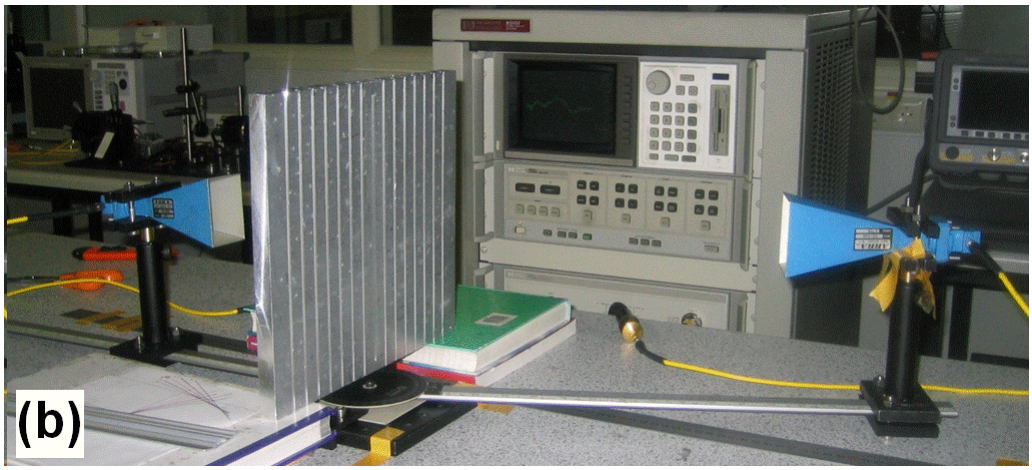

Fig. 4.1: (a) Schematic diagram of the transmission measurement setup. The setup consists of the network analyzer, two horn antennas and rotating arms. (b) Photograph of the transmission measurement setup.

4.1.2 Setup for Reflection Measurements

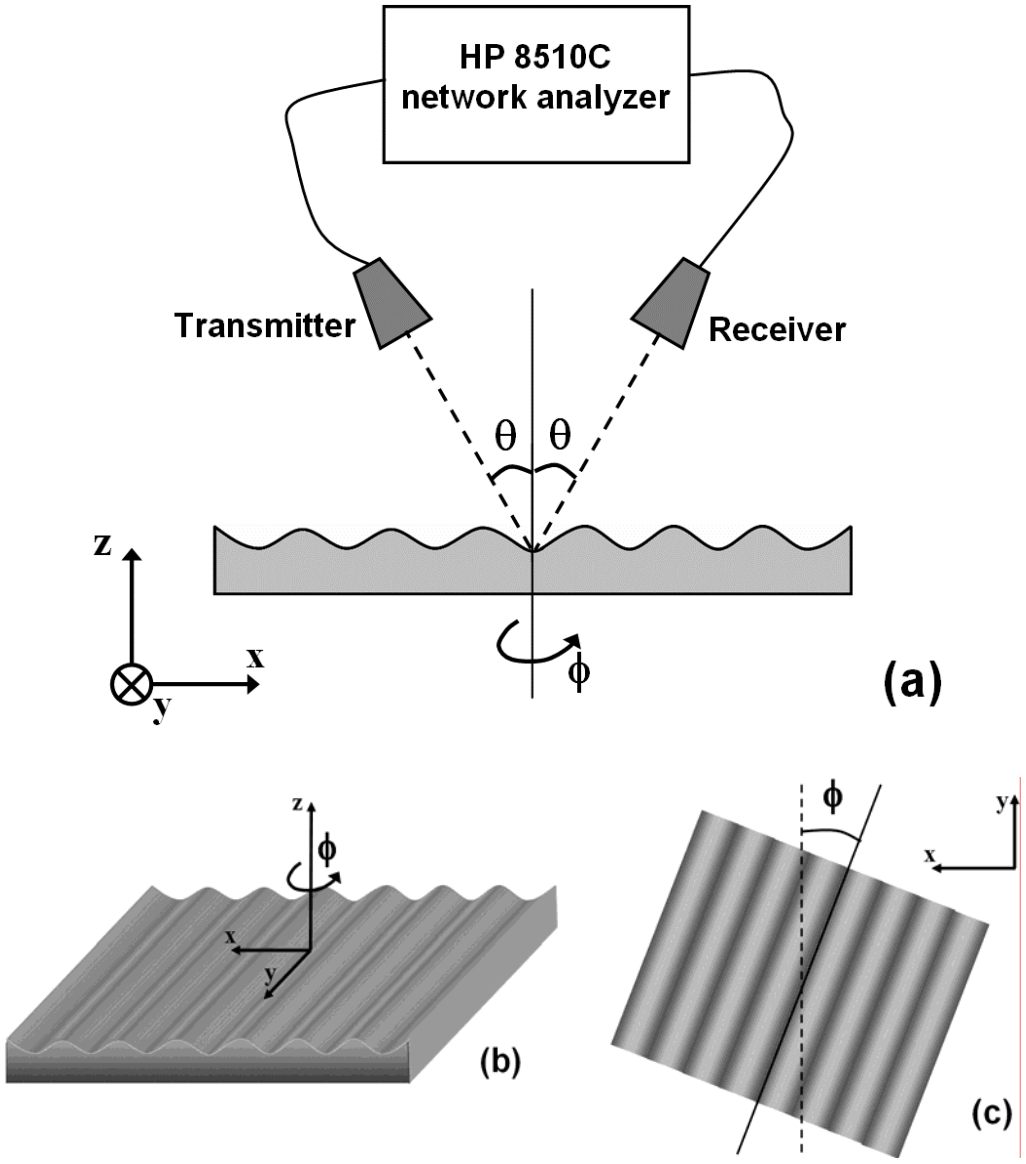

Fig. 4.2: (a) Schematic diagram of the reflection measurement setup (b) 3-D diagram of reflection sample (c) Description of azimuthal angle.

Figure 4.2 shows the setup we used in the reflection measurements. In these experiments, both antennas were attached to the rotating arms at a distance of 30 cm to the sample. Radiation was incident on the sample's surface with the polar angle θ. The receiver antenna was directed to the sample with the same angle at the opposite side of the sample's normal. To investigate the azimuthal angle (ϕ) dependence of sample reflectivity, the sample was rotated around its axis. The polar and azimuthal angles are shown in Fig. 4.2.

4.2 Transmission Measurements

Transmission intensity and directivity of samples in the far field were investigated. The experimental setup was explained in the previous section. For measuring the transmission intensity, receiver antenna was placed 20 cm away from the sample, receiver antenna was placed 30 cm (~20λ) away from the back surface. The incident field was in TM mode and always incident normally to the sample.

To measure the directivity, transmission intensities were measured by changing the collection angle. The receiver antenna was attached to a rotating arm and the angle was altered by one-degree increments.

4.1.1 Reference Sample: Slit without grating

To see the enhancement and directivity effect of grating samples, the first slit aperture without grating was analyzed as a reference. The transmission spectrum was measured between 10-37.5 GHz (8-30mm). Slit width was 2mm. As it is seen in Fig. 4.3 the transmitted beam through the slit was ~ 2% of the input radiation.

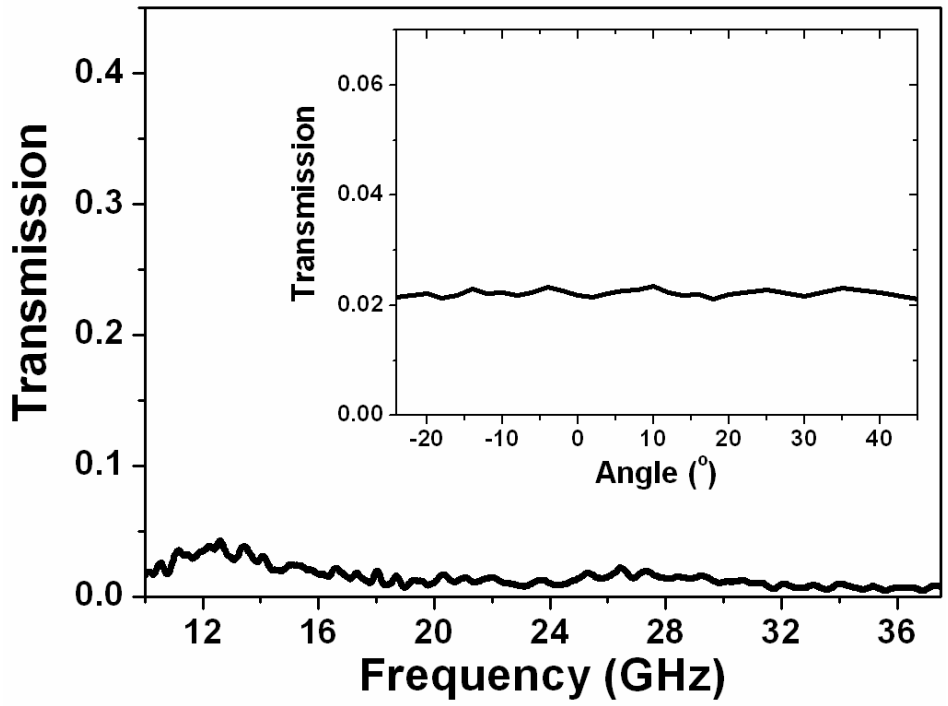

Fig. 4.3: Measured spectral transmission of the reference structure. Inset shows the angular dependence of the transmitted intensity measured at 15 GHz.

Exiting radiation was fully diffracted at all wavelengths. Inset figure shows the transmission intensity versus receipt angle at 15 GHz (a=λ/10) as an example. Transmission intensity was almost the same through −30°to 45°.

As a result, through a subwavelength slit aperture, the transmission was low and fully diffracted.

4.1.2 One-Sided Grating

To achieve better results we added a sinusoidal grating pattern on one side of the sample. To observe the effect of grating on transmission as well as the directivity, the results will be given under two topics in this section:

Grating on Front Surface:

In these measurements, the sample was placed so that the grating structure was on the illuminated side. In the transmission spectrum a peak was observed at 15.1 GHz (Fig. 4.4). Transmission intensity at peak value was ~8%. Enhancement was calculated as the ratio of transmission intensity of this sample to the transmission intensity of slit aperture. The enhancement factor is ~4 at the resonant frequency. Figure 4.5 shows the calculated spectral enhancement factor for this structure. However, the enhancement versus frequency plot was not confined to a specific frequency. Transmission data were recorded through the receipt angle −30º to 45º at 15.6 GHz. The beam radiated uniformly in all directions (Fig 4.6).

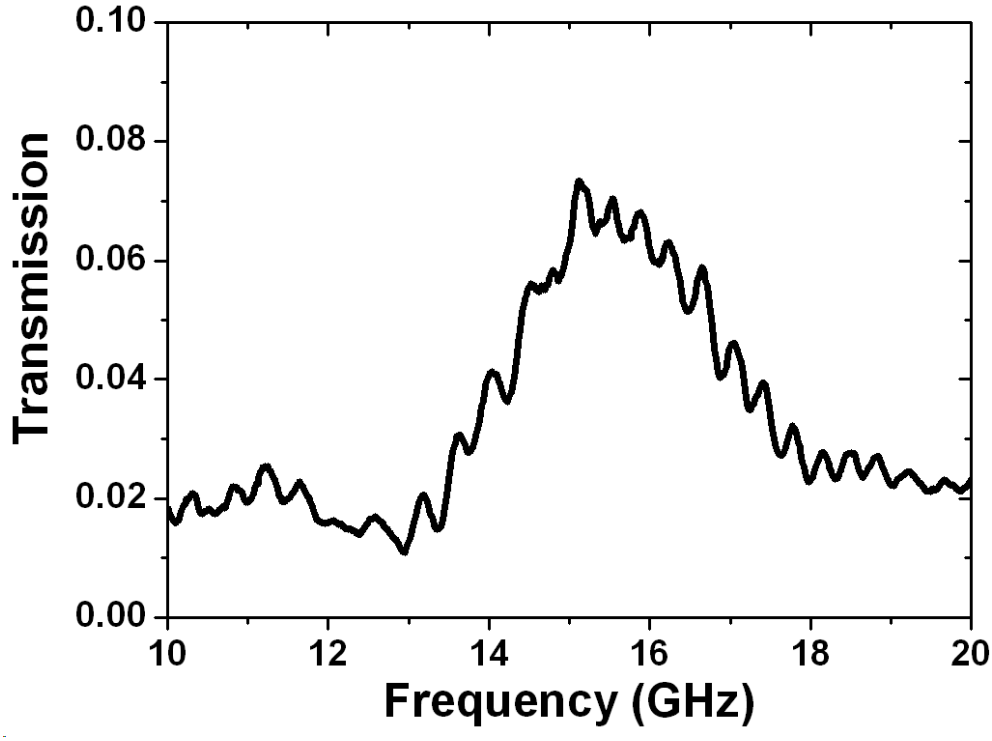

Fig. 4.4: Spectral transmission measurement of front-side grating structure.

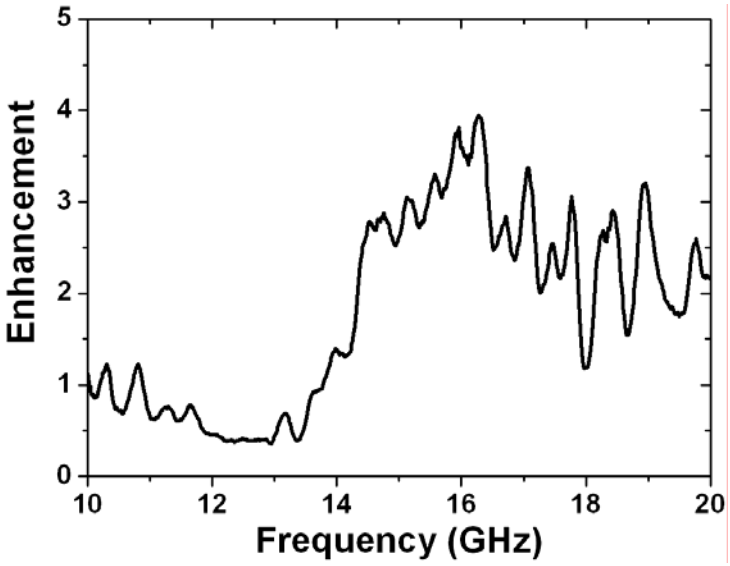

Fig. 4.5: Spectral enhancement factor obtained with the front-side grating structure

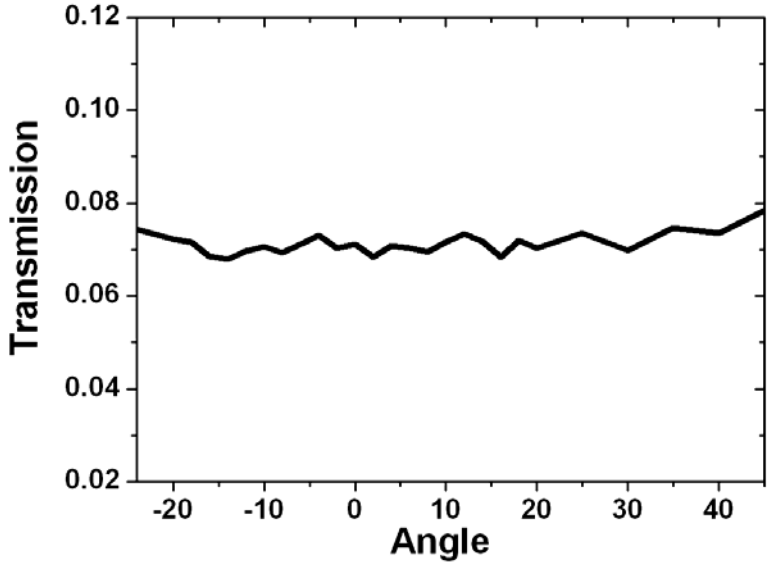

Fig. 4.6: Angular transmission spectrum of front-side grating structure.

Grating on Back Surface:

The same sample was used but it was placed so that the grating structure was on the exit side, illuminated face was not patterned. As seen in Fig. 4.7, a slightly blue-shifted transmission peak was observed at 16.1 GHz. The transmission intensity was ~10%, which is a bit higher than the intensity of front grating. The enhancement factor is above 6 at the resonant frequency (Fig. 4.8).

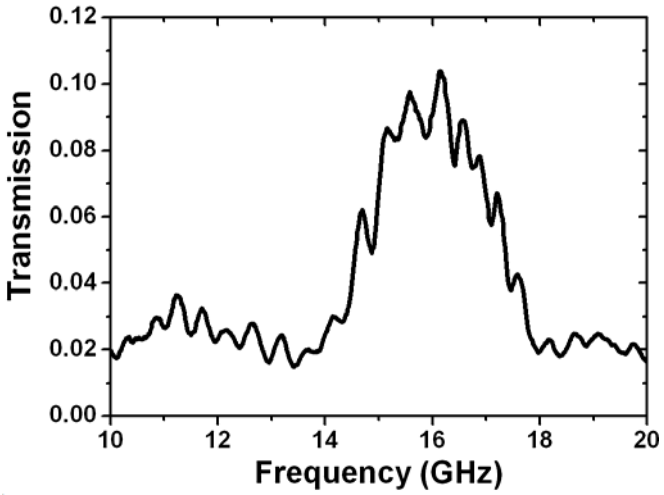

Fig. 4.7: Measured transmission spectrum of the back-side grating structure.

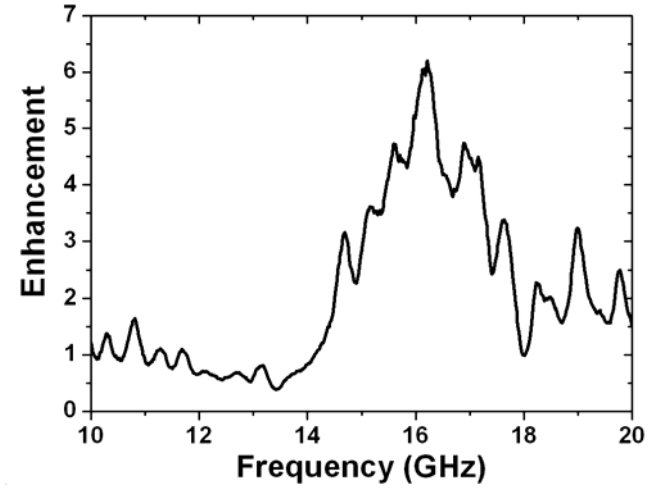

Fig. 4.8: Spectral enhancement of transmission in the back-side grating structure.

By recording the transmission intensity at various angles a strong angular dependence was observed. Figure 4.9 shows the angular transmission spectrum. The intensity versus angle plot implied that the transmitted light emerged in the shape of a well-defined beam with an observed full-width-half-maximum (FWHM) of 8º.

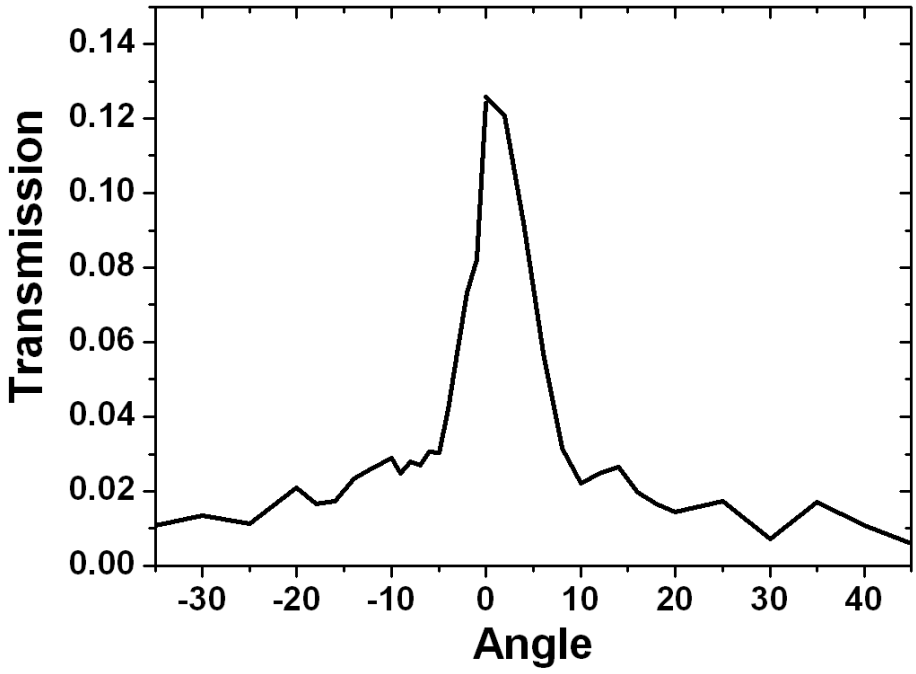

Fig. 4.9: Transmission at 16.1 GHz as a function of the receiver angle.

It was clear that while grating on the illuminated (front) face enhances the transmission by improving the coupling-in efficiency, grating on the back face gives directionality to the beam.

4.1.3 Double-Sided Gratings

As a result of the previous section, to achieve high transmission efficiency and directivity, grating should be on both sides of the sample. In this section, the

transmission spectrum and directivity measurements of double-side gratings are presented.

4.1.3.1 Sinusoidal Grating

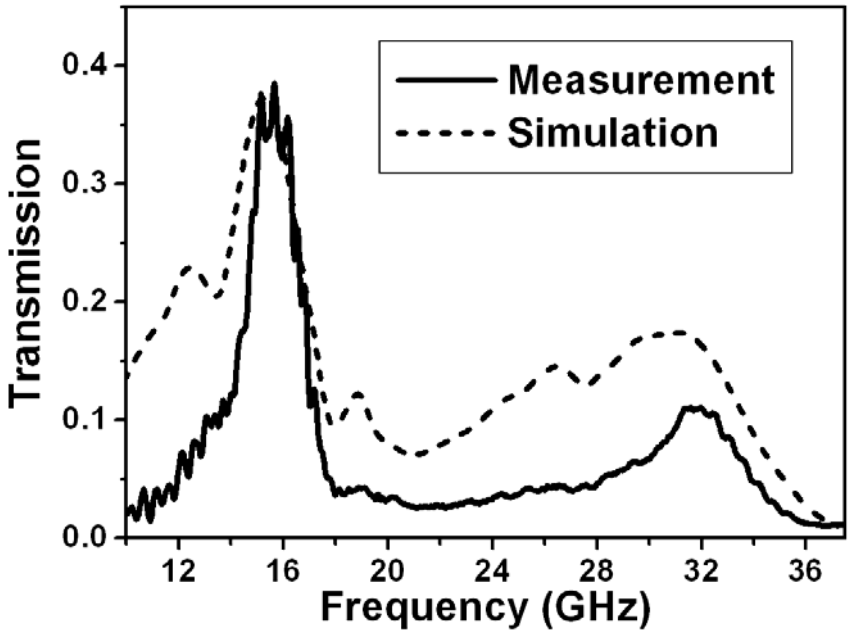

Fig. 4.10: Experimental and theoretical spectral transmission curves obtained with the double-sided sinusoidal grating sample.

Experimental and simulation results of transmission spectra of sinusoidal grating are shown in Fig. 4.10. The experimental results were in good agreement with our theoretical calculations. Two transmission peaks were measured at 15.6 GHz and 31.6 GHz frequencies, with amplitudes of 0.37 and 0.11 respectively. Theoretical simulations predicted slightly red-shifted similar transmission peaks: 37% at 15.2 GHz and 17% at 31.1 GHz. Coupling of incident radiation to the surface plasmon waves on the grating structure was given by the following equations:

$$\mathbf{k}_{SP} = n_d \mathbf{k}_0 \sin\theta \pm N\mathbf{k}_g \qquad (4.1)$$

$$k_{SP} = k_0 \sqrt{\frac{\varepsilon_m \varepsilon_d}{\varepsilon_m + \varepsilon_d}} \tag{4.2}$$

For microwave frequencies permittivity of metals are really high (~10^6), compared to the permittivity of air; so k_{SP} is close to k_0 in this range. Since the radiation is normally incident to the grating, the coupled wave vector should be in multiples of $\mathbf{k}_g$. In our sample λ_g was 16 mm and coupled frequencies were expected to be about c/λ_g = 18.75 GHz and integer multiples. However, in our experiments and simulations, the coupled frequencies shifted to lower frequencies (15.6, 31.6 GHz) due to the retardation by metal [17]. A maximum enhancement factor of ~20 was achieved around the first resonance frequency, which is shown in Fig. 4.11.

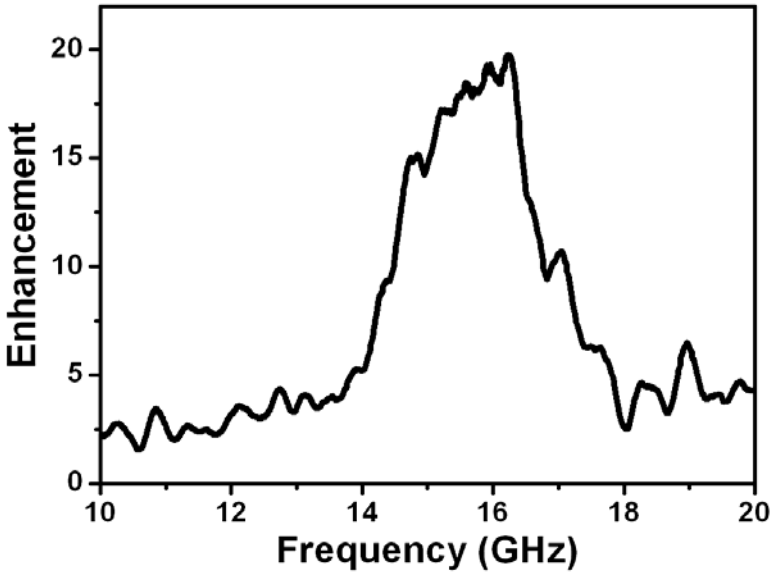

Fig. 4.11: Measured spectral enhancement factor of double-sided sinusoidal grating sample.

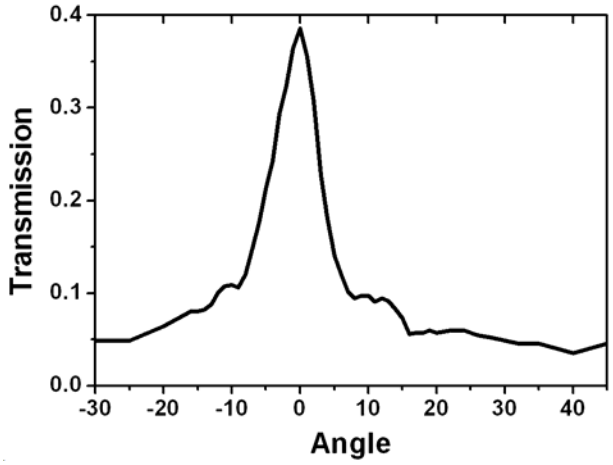

Fig. 4.12: Angular dependence of transmitted peak intensity for the double-sided sinusoidal grating sample.

The angular dependence of the transmitted peak intensity was measured. The resulting angular transmission spectrum is shown in Fig. 4.12. The transmission intensity was measured by changing the output collection angle. It was observed that, the transmission spectra were angle-dependent. In Fig. 4.13 transmission spectra were measured at angles 0º, 10º, 20º and 30º and are subsequently compared. The transmission peak shifted to lower frequencies and the intensity decreased by increasing the angle.

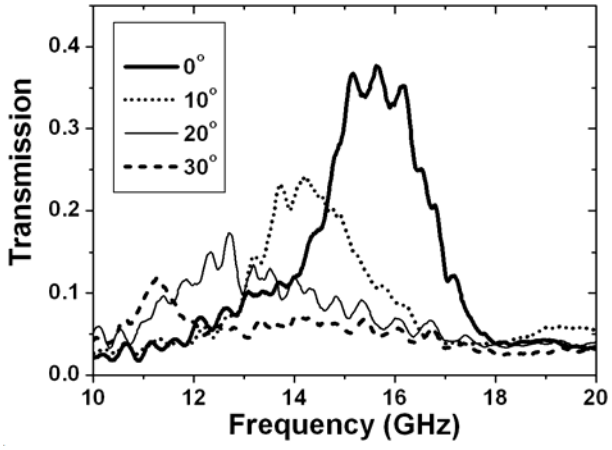

Fig. 4.13: Measured transmission spectra at different receiver angles.

These results implied that at a certain frequency the radiation emerged with maximum intensity at a particular angle from the surface. To confirm this statement, the transmission intensity as a function of the output angle was measured at different frequencies. For example the maximum intensities at 15.6 GHz, 14.1 GHz and 12.3 GHz were measured at angles 0º, ±10º and ± 20º, respectively (Fig. 4.14).

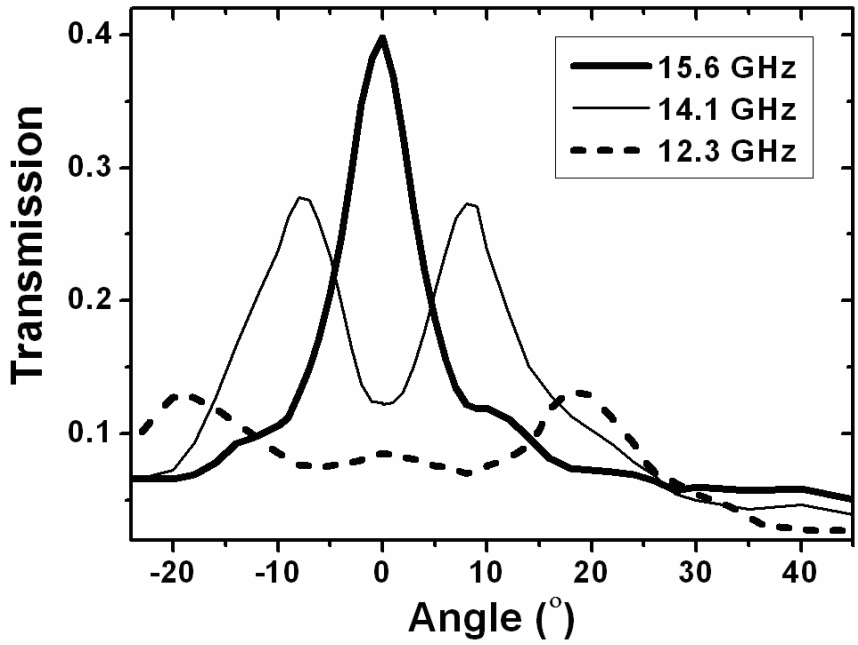

Fig. 4.14: Variance of transmission intensity as a function of output angle, measured at corresponding peak frequency values.

Theoretical diffraction analysis using the diffraction grating equation,

$$\theta_F^{(n,\pm)}(\lambda) = \sin^{-1}\left(\frac{n\lambda}{\lambda_g} \pm 1\right) \tag{4.3}$$

confirmed our measurement results when the blue-shift due to metal retardation is taken into account.

4.1.3.2 Symmetric Rectangular Grating

Measured and simulated transmission spectrum of the sample with double-sided symmetric rectangular grating is seen in Fig. 4.15. There were two resonance peaks, in which the first one was at 14.6 GHz with 45% transmission efficiency. The theoretical results were in good agreement with the experimental results. When compared with the sinusoidal structure, the transmission efficiency of this sample was higher and red-shifted about 1 GHz. A broader transmission peak was measured with this sample. An enhancement factor of 20.5 was achieved at 14.6 GHz. The spectral transmission enhancement is shown in Fig. 4.16.

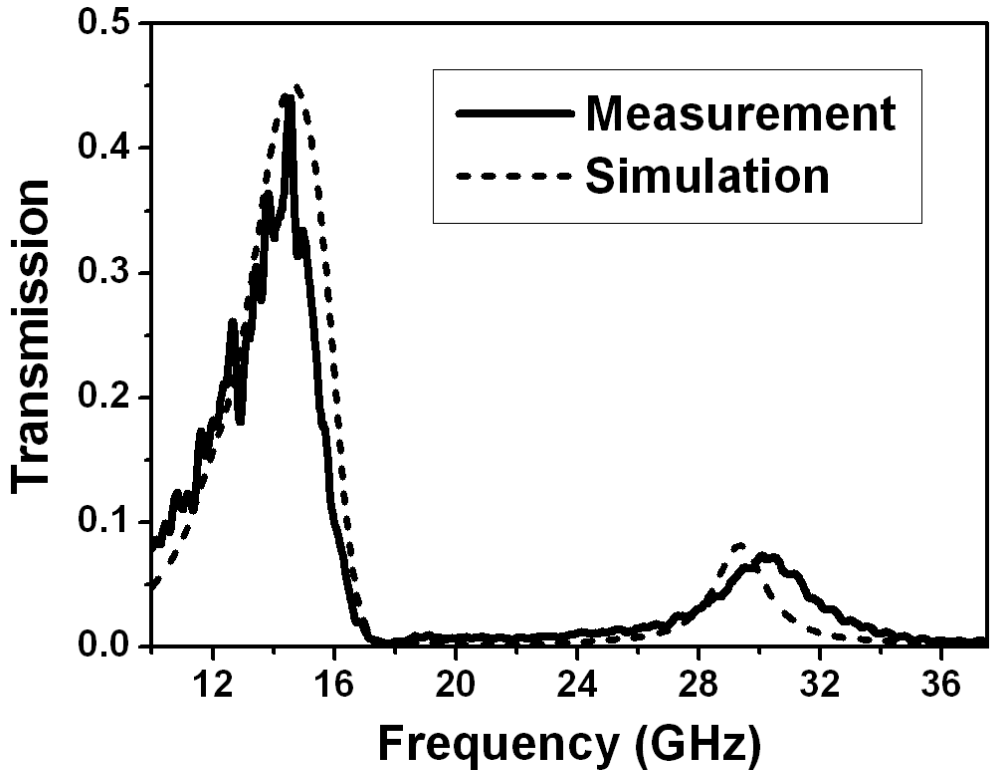

Fig. 4.15: Measured and calculated transmission spectrum for sample with double-sided symmetric rectangular grating.

To measure the directivity of this sample, an angular scan was carried out. Fig. 4.17 shows the directivity of the sample. The peak displayed a peak width of 13° FWHM.

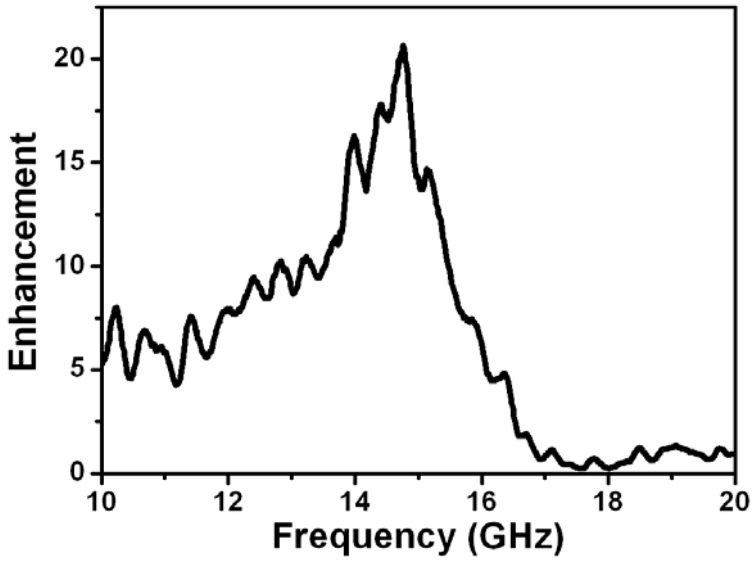

Fig. 4.16: The enhancement spectrum achieved with double-sided symmetric rectangular grating structure.

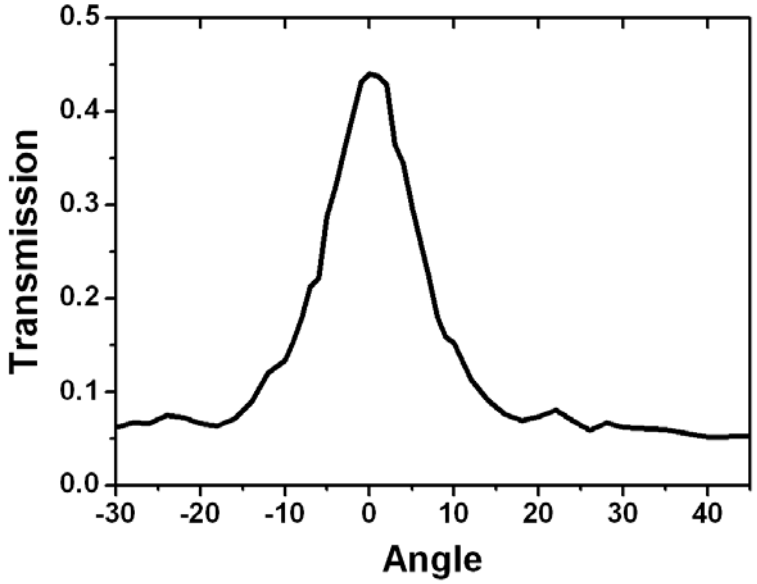

Fig. 4.17: The transmitted intensity as a function of the measurement angle.

The transmission intensity was measured by changing the output collection angle. It was observed that, the transmission spectra were angle-dependent. In Fig. 4.18 transmission spectra were measured at angles 0º, 10º, 20º and 30º and are subsequently compared. The transmission peak shifted to lower frequencies and the intensity decreased by increasing the angle.

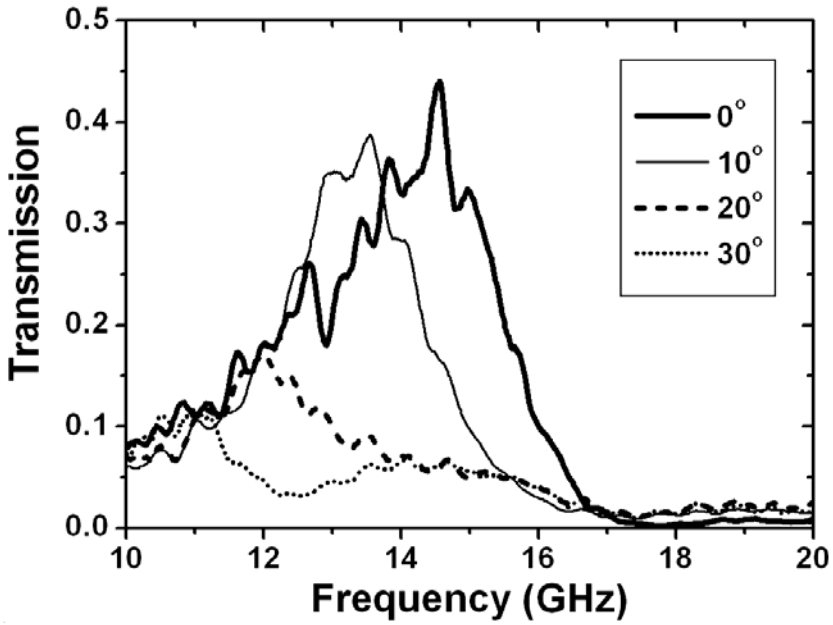

Fig. 4.18: Transmission spectra as a function of the receiver angle.

4.1.3.3 Asymmetric Rectangular Grating

Theoretical and experimental transmission spectra for this sample are given in Fig. 4.19. The results of this structure were more promising since the transmission peak was higher and narrower. Resonance frequency was at 14.5 GHz, which is very close to the resonance frequency of symmetric rectangular structure. Transmission efficiency was ~50%, which was higher than the theoretically predicted peak transmission efficiency. The enhancement factor

was higher, about 25, and confined to the resonant frequency (Fig. 4.20). When we compared this with the other structures, the enhancement plots of sinusoidal and symmetric rectangular were broader so that enhancement occurred within a broader frequency range. However, with asymmetric square grating, enhancement was confined to a certain frequency determined by the period. Hence this type of asymmetric grating is more useful for applications where wavelength selectivity is important.

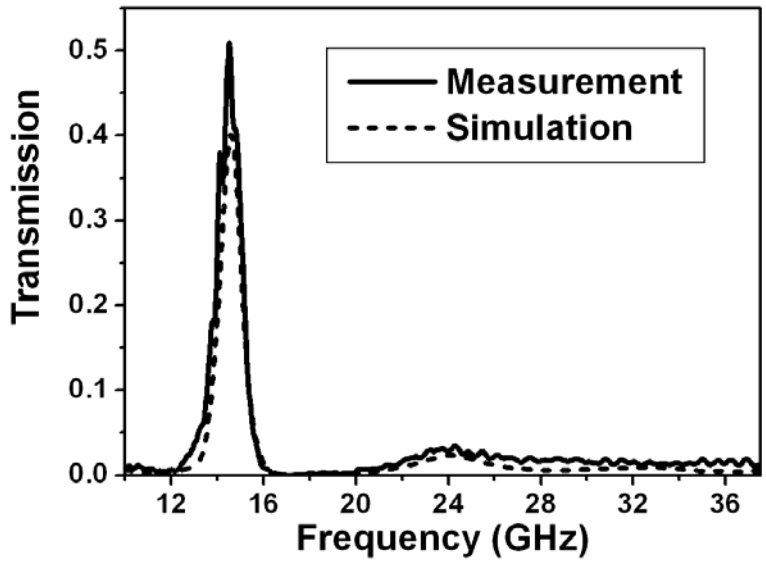

Fig. 4.19: Measured and simulated transmission spectrum for the sample with double-sided asymmetric rectangular grating.

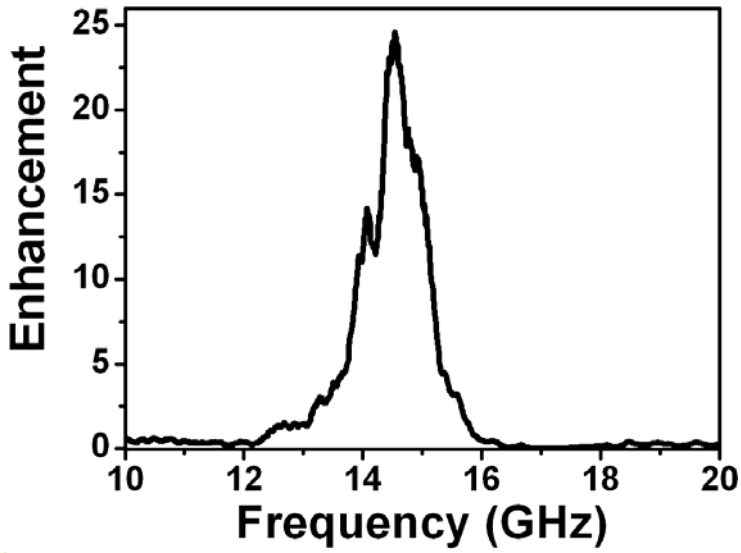

Fig. 4.20: Enhancement spectrum of double-sided asymmetric rectangular grating structure.

Figure 4.21 shows the transmission intensity as a function of the output collection angle. The measured FWHM divergence of peak was 8°. The directivity was higher compared to other samples.

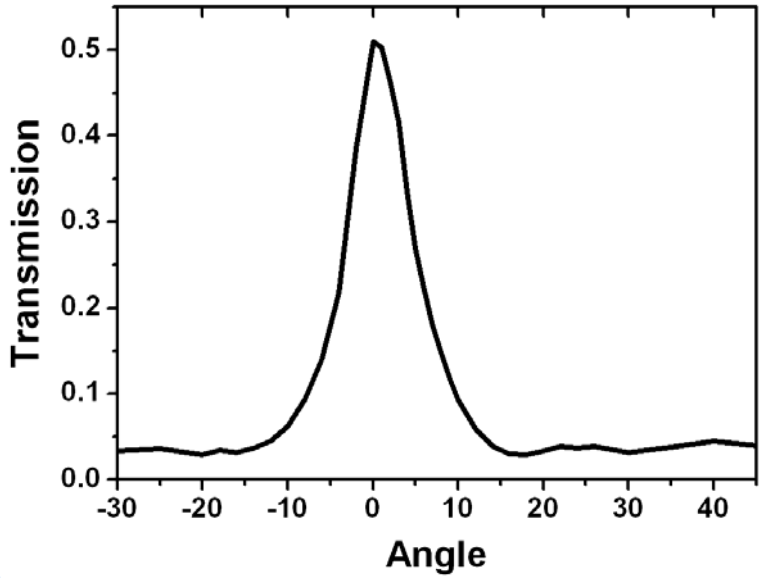

Fig. 4.21: Directivity measurement of the sample with double-sided asymmetric square grating.

A summary of transmission measurement results is presented in Table 4.1.

Sample	SP Resonance Frequency	Peak Transmission	Enhancement	FWHM
Reference	–	4%	–	–
One-sided grating (front-illuminated)	15.1 GHz	8%	~4	–
One-sided grating (back-illuminated)	16.1 GHz	10%	~6	8°
Double-sided sinusoidal grating	15.6 GHz	37%	~20	9°
Double-sided symmetric rectangular grating	14.6 GHz	45%	~21	13°
Double-sided symmetric rectangular grating	14.5 GHz	51%	~25	8°

4.2 Reflection Measurements

Reflection measurements were done in the 7.5–15 mm wavelength region which corresponds to the microwave spectrum of 20–40 GHz. The one-sided sinusoidal grating sample with a 16 mm grating period was measured in s-s and p-p configuration. The outcoupling/re-radiation of SP waves was investigated by the observation of a reflected field. Reflectivity peaks were observed around

the SP resonance wavelengths. A good agreement was achieved with the theoretical calculations.

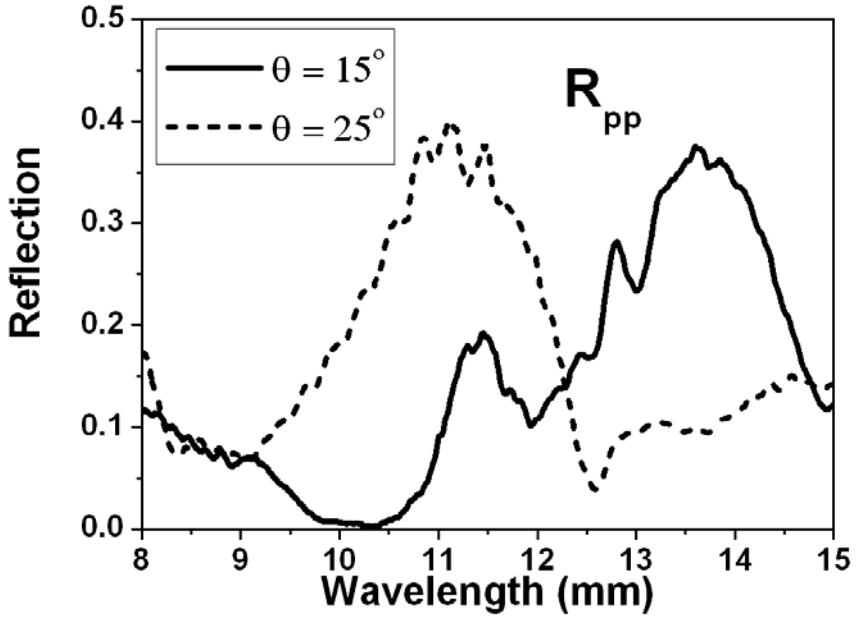

Fig. 4.22: Reflectivity (R_{pp}) measurement under different illumination conditions. SP resonance (reflectivity peak) blue-shifts for higher θ values.

Using the scalar SP coupling condition we can find the grating-coupled resonant SP mode:

$$k_{SP} = k_0 \sin\theta \cos\phi \pm N k_g \tag{4.4}$$

where N is an integer, and $k_0 \sin\theta \cos\phi$ is the projection of the wave vector of the incident radiation along the grating axis. Different SP modes will be excited under different illumination conditions which depend on the θ and ϕ values. As θ is increased, SP-coupling should occur at shorter wavelengths. An inverse relation was expected for the ϕ-dependence. Using the assumption that $k_{SP} \approx k_0$ in microwave spectrum for metallic layers and converting Eq. (4.3) in terms of wavelengths we obtain:

$$\lambda_{SP} = \frac{\lambda_g (1 - \sin\theta\cos\phi)}{N} \tag{4.5}$$

Figure 4.22 shows the measured reflectivity spectrum (R_{pp}) under two different illumination conditions: (θ,ϕ) = (15°, 0°), and (θ,ϕ) = (25°, 0°). Reflectivity peaks at ~13.6 mm and ~11.2 mm were measured for θ = 15° and θ = 25°, respectively. Theoretical λ_{SP} values for these illumination conditions (N = 1) were calculated as 11.86 mm and 9.24 mm. Hence, the experimental SP resonance was red-shifted by ~2 mm. Such a red-shift was expected due to the retardation effect introduced by the metallic grating layer [17]. A similar red-shift was also observed in our transmission measurements.

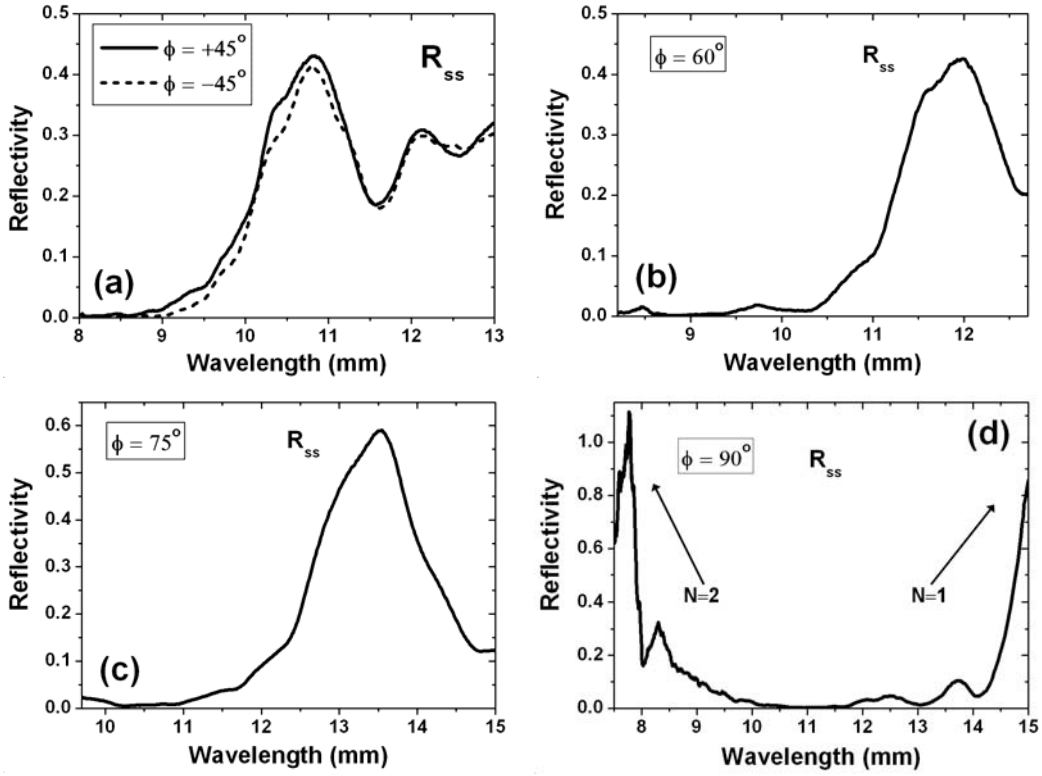

Fig. 4.23: Reflectivity measurements of the sinusoidal grating sample in the s-s configuration. (a) $\phi = \pm 45°$, (b) $\phi = 60°$, (c) $\phi = 75°$, (d) $\phi = 90°$.

Figure 4.23 shows the reflectivity (R_{ss}) measurements as a function of ϕ ($\theta =$ 30° for all of the measurements). The SP resonance red-shifted for larger ϕ values. Very similar reflectivity peaks were obtained for $\phi = +45°$ and $\phi = -45°$ (Fig. 4.23(a)). The first order (N = 1) coupling modes were observable within the measurement range. Higher order modes were below the short-wavelength limit (7.5 mm) of the measurement setup. Only for $\phi = 90°$, could the second order SP coupling be observed around 8 mm (Fig. 4.23(d)).

Table 4.1 shows the measured and calculated SP coupling wavelengths (λ_{SP}) as a function of the ϕ value. A close agreement between the experimental and theoretical values was achieved. The first order SP peak for $\phi = 90°$ could not be observed, however, the increasing reflectivity intensity towards 15 mm shows a strong sign of a peak around 16 mm.

Illumination Condition	**Theoretical Calculation**	**Experiment**
$(\theta, \phi) = (30°, 45°)$	$\lambda_{SP} = 10.34$ mm	$\lambda_{SP} \sim 10.8$ mm
$(\theta, \phi) = (30°, 60°)$	$\lambda_{SP} = 12$ mm	$\lambda_{SP} \sim 12.0$ mm
$(\theta, \phi) = (30°, 75°)$	$\lambda_{SP} = 13.93$ mm	$\lambda_{SP} \sim 13.6$ mm
$(\theta, \phi) = (30°, 90°)$	$\lambda_{SP} = 16$ mm ($N = 1$)	$\lambda_{SP} > 15$ mm ($N = 1$)
	$\lambda_{SP} = 8$ mm ($N = 2$)	$\lambda_{SP} \sim 7.8$ mm ($N = 2$)

Table 4.1: Measured and calculated SP coupling wavelengths under different illumination angles.

To compare measurements in s-s and p-p configuration, R_{ss} and R_{pp} curves measured under the $(\theta,\phi) = (30°, 45°)$ illumination condition, are shown in Fig. 4.24. Very similar results were obtained for both measurement configurations. Reflectivity peaks around the same λ_{SP} wavelength with very close peak intensity was observed.

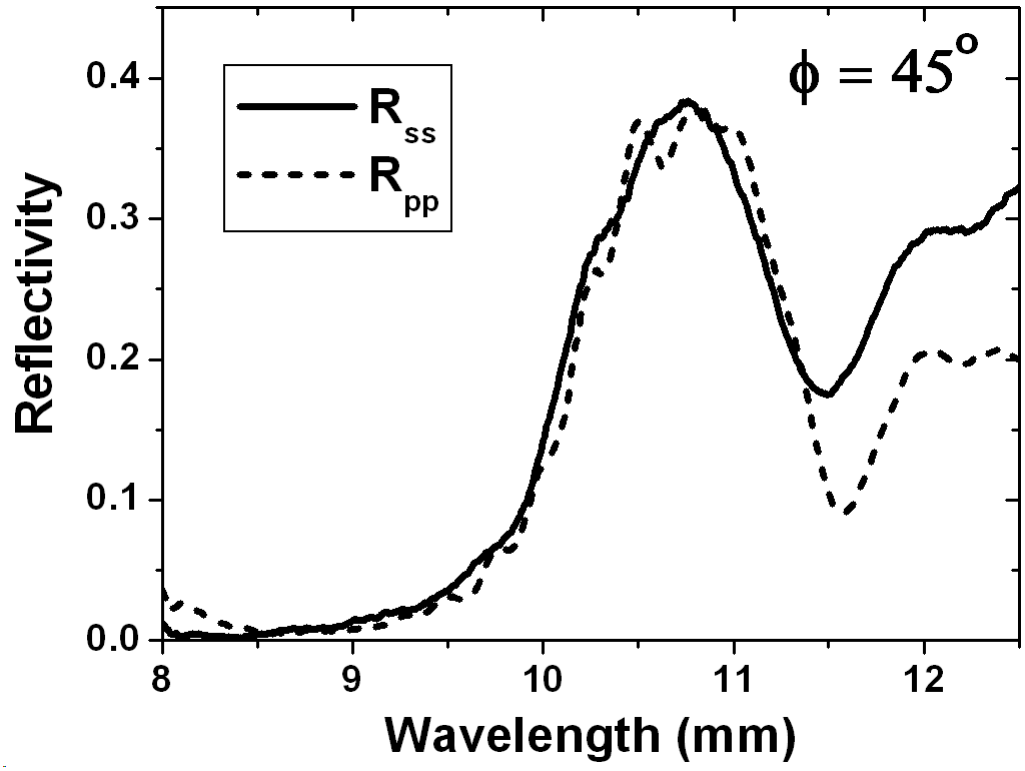

Fig. 4.24: Measured reflectivity curves for s-s (R_{ss}) and p-p (R_{pp}) measurement configurations. Measurement was conducted at (θ,ϕ) = (30^o, 45^o).

Chapter 5

Conclusion

In conclusion, we have analyzed the coupling mechanism between microwave radiation and surface plasmons in 1-D metallic grating structures. Enhanced transmission was demonstrated through subwavelength (~λ/10) apertures surrounded by metallic gratings on both surfaces. Several grating geometries were studied in the transmission experiments. Spectral reflection measurements under different angular conditions resulted in reflectivity peaks around the SP resonance wavelengths. The theoretical simulations and analytical calculations were in good agreement with the experimental results.

Our transmission experiments showed that periodic surface corrugation led to enhanced transmission and beaming around SP resonance frequency, which was determined by the groove periodicity. Both grating sides were responsible for transmission enhancement, whereas only the back-side grating was in charge of the directivity of the transmitted field. All three double-sided grating samples exhibited >20 enhancement factors, along with directivities of <10°. The best results were obtained with the asymmetric rectangular grating structure. An absolute transmission of 51% at 14.5 GHz was measured, which corresponded to an enhancement of 25. These results were in good agreement with our simulations, which predicted 40% transmission and 20 enhancement at 14.5 GHz.

Reflection measurements showed close agreement with our theoretical predictions. The grating-coupling phenomenon that was in the microwave spectrum was verified by these experiments. Reflectivity peaks were obtained at the SP resonance wavelengths. Polar and azimuthal angular scan data showed very close agreement with the analytical calculations.

We also designed and measured 2-D grating structures with subwavelength single-hole apertures during our study. However, we were not able to observe enhanced transmission with these structures. We were not able to simulate 2-D structures with our simulation tools. To understand the enhancement mechanism of 2-D structures, appropriate 2-D simulations should be carried out.

For future research directions, further study should be devoted to 2-D structures. The ultimate goal should be to move this work toward optical wavelengths.

List of Publications

1) S. Akarca-Biyikli, Irfan Bulu, and E. Ozbay, "Enhanced transmission of microwave radiation in one-dimensional metallic gratings with sub-wavelength aperture," accepted for publication in 16 August 2004 issue of *Applied Physics Letters* .

2) S. Akarca-Biyikli, Irfan Bulu, and E. Ozbay, “Resonant Excitation of Surface Plasmons in One-Dimensional Metallic Grating Structures at Microwave Frequencies,” submitted to *Journal of Optics A*: *Pure and Applied Optics* , Special Issue on 'Nanostructured Optical Meta-Materials: Beyond Photonic Bandgap Effects (2004).

Bibliography

[1] V. M. Agranovich and D. L. Mills, *Surface Polaritons: Electromagnetic Waves at Surfaces and Interfaces*, North-Holland, Amsterdam, 1982.

[2] H. Raether, *Surface Plasmons on Smooth and Rough Surfaces and on Gratings*, Springer-Verlag, Germany, 1988.

[3] D. R. Tilley, "Basic surface plasmon theory," in *Surface Plasmon-Polaritons*, IOP Publishing , Bristol, 1988

[4] A. D. Boardman and T. Twardowski, "Nonlinear surface plasmon-polaritons," in *Surface Plasmon-Polaritons*, IOP Publishing , Bristol, 1988

[5] J. E. Sipe and G. I. Stegeman, "Nonlinear optical response of metal surfaces," in *Surface Polaritons*, V. M. Agranovich and D. L. Mills, Ed. North-Holland, Amsterdam, 1982

[6] S. Ushioda and R. Loudon, "Raman scattering by surface polaritons," in *Surface Polaritons*, V. M. Agranovich and D. L. Mills, Ed. North-Holland, Amsterdam, 1982

[7] A. Nemetz, U. Fernandez, and W. Knoll, "Surface plasmon field-enhanced Raman spectroscopy with double gratings," *J. Appl. Phys*., vol. 75, pp. 1582-1585, 1994.

BIBLIOGRAPHY

[8] T. W. Ebbesen, H. J. Lezec, H. F. Ghaemi, T. Thio, and P.A Wolf, "Extraordinary optical transmission through sub-wavelength hole arrays," *Nature (London),* vol. 391, pp. 667-669, 1998.

[9] H. A. Bethe, "Theory of diffraction by small holes," *Phys. Rev.,* vol. 66, pp. 163–182, 1944.

[10] D. E. Grupp, H. J. Lezec, T. W. Ebbesen, K. M. Pellerin, and T. Thio, "Crucial role of metal surface in enhanced transmission through subwavelength apertures," *Appl. Phys. Lett.,* vol. 77, pp. 1569-1571, 2000.

[11] F. J. Garcia-Vidal, L. Martin-Moreno, H. J. Lezec, and T. W. Ebbesen, "Focusing light with a single subwavelength aperture flanked by surface corrugations," *Appl. Phys. Lett.,* vol. 83, pp. 4500-4502, 2003.

[12] F. J. Garcia-Vidal, H. J. Lezec, T. W. Ebbesen, and L. Martin-Moreno, "Multiple paths to enhance optical transmission through a single subwavelength slit," *Phys. Rev. Lett.,* vol. 90, pp. 213901-1-213901-4, 2003.

[13] W. Liu and D. P. Tsai, "Optical tunneling effect of surface plasmon polaritons and localized surface plasmon resonance," *Phys. Rev. B,* vol. 65, pp. 155423-1-155423-6, 2002.

[14] J. A. Porto, F. J. Garcia-Vidal, and J. B. Pendry, "Transmission resonances on metallic gratings with very narrow slits," *Phys. Rev. Lett.,*

vol. 83, pp. 2845-2848, 1999.

[15] A. Barbara, P. Quémarais, E. Bustarret, and T. Lopez-Rios, "Optical transmission through subwavelength metallic gratings," *Phys. Rev. B,* vol. 66, pp. 161403-1-161403-4, 2002.

[16] J. M. Steele, C. E. Moran, A. Lee, C. M. Aguirre, and N. J. Halas, "Metallodielectric gratings with subwavelength slots: Optical properties," *Phys. Rev. B*, vol. 68, pp. 205103-1-205103-7, 2003.

[17] H. J. Lezec, A. Degiron, E. Devaux, R. A. Linke, L. Martin-Moreno, F. J. Garcia-Vidal, and T. W. Ebbesen, "Beaming light from a subwavelength aperture," *Science,* vol. 297, pp. 820-822, 2002.

[18] L. Martin-Moreno, F. J. Garcia-Vidal, H. J. Lezec, A. Degiron, and T. W. Ebbesen, "Theory of Highly Directional Emission from a Single Subwavelength Aperture Surrounded by Surface Corrugations," *Phys. Rev. Lett.,* vol. 90, pp. 167401-1-167401-4, 2003.

[19] Y. Takakura, "Optical resonance in a narrow slit in a thick metallic screen," *Phys. Rev. Lett.,* vol. 86, pp. 5601-5603, 2001.

[20] D. E. Grupp, H. J. Lezec, T. Thio, and T. W. Ebbesen, "Beyond the Bethe Limit: Tunable Enhanced Light Transmission Through a Single Sub-Wavelength Aperture," *Adv. Mater.,* vol. 11, pp. 860-862 1999.

[21] D. E. Grupp, H. J. Lezec, T. W. Ebbesen, K. M. Pellerin, and T. Thio, "Crucial role of metal surface in enhanced transmission through subwavelength apertures," *Appl. Phys. Lett.,* vol. 77, pp. 1569-1571,

2000.

[22] L. Martin-Moreno, F. J. Garcia-Vidal, H. J. Lezec, K. M. Pellerin, T. Thio, J. B. Pendry and T. W. Ebbesen, "Theory of Extraordinary Optical Transmission through Subwavelength Hole Arrays," *Phys. Rev. Lett.*, vol. 86, pp. 1114-1117, 2001.

[23] H. F. Ghaemi, T. Thio, D. E. Grupp, T. W. Ebbesen, and H. J. Lezec, "Surface plasmon enhance optical transmission through subwavelength holes," *Phys. Rev. B*, vol. 58, pp. 6779-6782, 1998.

[24] E. Popov, M. Neviere, S. Enoch, and R. Reinisch, "Theory of light transmission through subwavelength periodic hole arrays," *Phys. Rev. B*, vol. 62, pp. 16100-16108, 2000.

[25] J. M. Vigoureux, "Analysis of Ebbesen experiment in the light of evanescent short range diffraction," *Opt. Commun.*, vol.198, pp. 257-263, 2001.

[26] N. Bonod, S. Enoch, L. Li, E. Popov, and M. Neviere, "Resonant optical transmission through thin metallic films with and without holes," *Opt. Exp.*, vol. 11, pp. 482-490, 2003.

[27] X. Shi and L. Hesselink, "Mechanisms for Enhancing Power Throughput from Planar Nano-Apertures for Near-Field Optical Data Storage," *J. Appl. Phys.*, vol. 41, pp. 1632-1635, 2002.

[28] J. G. Rivas, C. Schotsch, P. H. Bolivar, and H. Kurz, "Enhanced transmission of THz radiation through subwavelength holes," *Phys. Rev.*

B vol. 68, pp. 201306, 2003.

[29] A. P. Hibbins, J. R. Sambles, and C. R. Lawrence, "Grating-coupled surface plasmons at microwave frequencies," *J. Appl. Phys.*, vol. 86, pp. 1791-1795, 1999.

[30] A. P. Hibbins, J. R. Sambles, and C. R. Lawrence, "The coupling of microwave radiation to surface plasmon polaritons and guided modes via dielectric gratings," *J. Appl. Phys.*, vol. 87, pp. 2677-2683, 2000.

[31] A. P. Hibbins, J. R. Sambles, and C. R. Lawrence, "Excitation of remarkably nondispersive surface plasmons on a nondiffracting, dual-pitch metal grating," *Appl. Phys. Lett.,* vol. 80, pp. 2410-2412, 2002.

[32] M. J. Lockyear, A. P. Hibbins, J. R. Sambles, and C. R. Lawrence, "Low angular-dispersion microwave absorption of a dual-pitch nondiffracting metal bigrating," *Appl. Phys. Lett.,* vol. 83, pp. 806-808, 2003.

[33] A. P. Hibbins, J. R. Sambles, and C. R. Lawrence, "Gratingless enhanced microwave transmission through a subwavelength aperture in a thick metal plate," *Appl. Phys. Lett.*, vol. 81, pp. 4661-4663, 2002.

[34] M. J. Lockyear, A. P. Hibbins, J. R. Sambles, and C. R. Lawrence, "Surface-topography-induced enhanced transmission and directivity of microwave radiation through a subwavelength circular metal aperture," *Appl. Phys. Lett.,* vol. 84, pp. 2040-2042, 2004.

[35] C. Kittel, *Introduction to Solid State Physics*, John Wiley & Sons, New York, 1996.

[36] M. M. Sigalas, C. T. Chan, K. M. Ho, and C. M. Soukoulis, *Phys. Rev. B*, vol. 52, pp. 11744, 1995.

[37] E. V. Alieva et al., *Appl. Spectr.*, vol. 51, pp. 584, 1997.

[38] A. Otto, *Z. Phys.*, vol. 216, pp. 398, 1968.

[39] E. Kretschmann and H. Raether *Z. Naturf.*, vol. 230, pp. 2135, 1968.